

Resonant vibrational excitation of CO₂ by electron impact: Nuclear dynamics on the coupled components of the ²Π_u resonance

C. W. McCurdy,^{1,2} W. A. Isaacs,³ H.-D. Meyer,⁴ and T. N. Rescigno¹

¹Lawrence Berkeley National Laboratory, Computing Sciences, Berkeley, California 94720

²Department of Applied Science, University of California, Davis, Livermore, California 95616

³Lawrence Livermore National Laboratory, Physics and Advanced Technologies, Livermore, California 94551

⁴Theoretisch Chemie, Universität Heidelberg, Im Neuenheimer Feld 229, D-69120 Heidelberg, Germany

(Received 3 December 2002; published 17 April 2003)

We report the results of a fully *ab initio* study of resonant vibrational excitation of CO₂ by electron impact via the 3.8 eV ²Π_u shape resonance. First, we solve the fixed-nuclei, electronic scattering problem using the complex Kohn variational method to produce resonance parameters for both the ²A₁ and ²B₁ components of the resonance for a variety of symmetric-stretch geometries and for a range of bending angles. The nuclear dynamics associated with the two components of the resonance are coupled by Renner-Teller coupling. We carry out a two-mode treatment of the nuclear dynamics in a complex local potential model using the complex resonance energy surfaces derived from our calculated fixed-nuclei cross sections with Renner-Teller coupling.

DOI: 10.1103/PhysRevA.67.042708

PACS number(s): 34.80.Gs

I. INTRODUCTION

Resonance enhancement of electron-CO₂ collision cross sections near 4-eV incident energy has been known and studied since the early work of Brücke [1]. Detailed studies of resonant vibrational excitation have been carried out by, among others, Čadež *et al.* [2], Johnstone, Akther, and Newell [3] and, most recently, by Allan [4,5]. While much of our thinking about resonant vibrational excitation is influenced by local complex potential theories, most notably the one-dimensional boomerang models of Birtwistle and Herzenberg [6] and Dubé and Herzenberg [7], there are aspects of electron-CO₂ scattering, as Currell and Comer [8] first pointed out, that have a polyatomic origin and cannot be described by a simple one-dimensional model.

CO₂ provides a serious challenge and test of theories of polyatomic resonant vibrational excitation for a number of reasons. First, there is the phenomenon known as *Fermi resonance*, which refers to an accidental degeneracy between certain vibrational modes [9]. This, in turn, gives rise to strong mixing among various zeroth-order vibrational states. Consequently, it is necessary to adopt a multidimensional treatment of the nuclear motion just to be able to describe the physical vibrational states of the target. This fact was illustrated in our previous *ab initio* study of electron-CO₂ scattering [10], in which we carried out a three-dimensional boomerang treatment of vibrational excitation using the complex ²A₁ potential surface derived from a series of fixed-nuclei variational scattering calculations. While those earlier calculations clearly showed the importance of treating both symmetric stretch and bending motion in the nuclear dynamics and were successful in reproducing the envelope of the resonant vibrational excitation cross sections for both members of the lowest Fermi dyad, they failed to reveal the detailed structure in the cross sections that is evident in Allan's [4] recent measurements.

The question of the origin of that structure in the cross

sections brings us to a second major problem, one which probes the fundamentally polyatomic nature of the collision dynamics and constitutes the major focus of this paper. The resonance enhancement of the excitation cross sections is due to the formation of a temporary (CO₂⁻) negative ion which, in linear geometry, has ²Π_u symmetry. Upon bending, this ²Π_u state splits into nondegenerate ²A₁ (lower) and ²B₁ (upper) components, the latter of which we ignored in our earlier treatment. Kazanskii [11], who has performed several calculations on the electron-CO₂ problem using model potentials, has recently given a description of the essential physics involved in treating the two-component resonance collision problem, but lacking substantive information about the resonance surfaces, he did not pursue the matter further. In an earlier study, Currell and Comer [8] had speculated that nonadiabatic coupling between the two components of the ²Π_u resonance could be responsible for resonant excitation of odd quanta of nontotally symmetric vibrational modes, which has also been observed. The present treatment, which includes both the ²A₁ and ²B₁ surfaces, shows this *not* to be the case but does reveal that the weak interference structure which Allan observed is a manifestation of this coupling.

This study takes a completely *ab initio* approach to resonant vibrational excitation of CO₂ and provides a more complete treatment of the nuclear dynamics than that presented in our earlier study [10]. The fixed-nuclei variational calculations [12] are extended to B₁ symmetry and used to construct a complex potential surface for the ²B₁ state of CO₂⁻. The nuclear dynamics problem is then solved by extending the time-dependent Boomerang model [13] to treat multidimensional motion on two resonance surfaces coupled by nonadiabatic (Renner-Teller) coupling. In the spirit of a complete first-principles approach, the target vibrational states, which were computed using degenerate perturbation theory in our earlier treatment [14], are numerically computed here using the calculated CO₂ potential surface. To complete the

treatment, we extend the analyses of Dubé and Herzenberg [7] and Estrada *et al.* [15] to derive an expression for the differential cross section within the coupled-channel boomerang model which permits a comparison of the *ab initio* results with Allan's absolute measurements.

The organization of this paper is as follows. The following section gives a brief summary of the complex Kohn methodology used to carry out the fixed-nuclei electron-scattering calculations and to calculate the resonance surfaces. In Sec. III we outline the extension of the multidimensional boomerang model to the case of coupled resonance states. Our treatment follows closely that of Estrada, Cederbaum, and Domcke [15], with extensions appropriate for a molecule belonging to a non-Abelian point group. The angular dependence of the excitation cross sections within the coupled-channel boomerang model is also derived. In Sec. IV we briefly review the Renner-Teller effect in linear triatomic molecules and show how this nonadiabatic coupling scheme applies to the present case of electron-scattering resonances. This section also presents the working equations used in the present study. In Sec. V, we discuss the numerical solution of the coupled-channel boomerang model using a time-dependent wave-packet approach. We also summarize our implementation using the multiconfiguration time-dependent Hartree (MCTDH) method [16]. Our results are presented in Sec. VI along with comparisons to experiment. We conclude, in Sec. VII, with a brief summary as well as a discussion of some of the open questions that remain, including the possible interaction of the resonance dynamics with the virtual state that may be responsible for producing structure in the vibrational excitation cross sections near threshold, as well as the mechanisms that may be responsible for exciting "forbidden" (odd-quanta) bending levels. Unless specified otherwise, we use atomic units throughout.

II. FIXED-NUCLEI ELECTRON-SCATTERING CALCULATIONS

A. Calculating the complex potential surfaces for the 2A_1 and 2B_1 components of the resonance

The fixed-nuclei calculations were carried out using the complex Kohn variational method. The details of calculations using this method for electron-CO₂ collisions were described in our first paper on the fixed-nuclei cross sections for this problem [12], which showed variations in the cross sections with the symmetric stretch coordinate. To understand the physical description of the resonance states, it is useful to recall the form of the trial wave function in these variational calculations. In the Kohn method, we use a stationary principle for the T matrix

$$T_{stat} = T_{trial} - 2 \int \Psi(H - E)\Psi, \quad (1)$$

which is evaluated with a trial wave function for the $(N + 1)$ -electron system of the form

$$\Psi = \mathcal{A}[\Phi_o(\vec{r}_1 \cdots \vec{r}_N)F(\vec{r}_{N+1})] + \sum_{\mu} d_{\mu} \Theta_{\mu}(\vec{r}_1, \dots, \vec{r}_{N+1}). \quad (2)$$

In Eq. (2) Φ_o is the Hartree-Fock, self-consistent field (SCF) ground state of CO₂, \mathcal{A} antisymmetrizes the coordinates of the incident electron with those of the target electrons and the sum contains square-integrable, $(N + 1)$ -electron terms that describe correlation and polarization effects. The scattering function $F(\vec{r}_{N+1})$ is further expanded in a combined basis of Gaussian (ϕ_i) and continuum (Ricatti-Bessel, j_l , and Hankel, h_l^+) basis functions

$$F(\vec{r}) = \sum_i c_i \phi_i(\vec{r}) + \sum_{lm} [j_l(kr) \delta_{l_0} \delta_{mm_0} + T_{l_0 mm_0} h_l^+(kr)] Y_{lm}(\hat{r}) / r. \quad (3)$$

Applying the stationary principle [Eq. (1)] results in a set of linear equations for the coefficients c_i , d_{μ} , and $T_{l_0 mm_0}$. The T -matrix elements $T_{l_0 mm_0}$ are the fundamental dynamical quantities from which all fixed-nuclei cross sections are derived.

To perform nuclear dynamics studies using the extension of the boomerang model to coupled resonances, we require the complex local potential surfaces formed by the resonance positions and widths as a function of nuclear geometry. Calculating accurate resonance parameters requires a proper description of the dynamic response of the target to the incident electron, and that effect is described by including asymptotically decaying closed channels in the trial wave function using the $\Theta_{\mu}(\vec{r}_1, \dots, \vec{r}_{N+1})$ terms in Eq. (2).

For the molecular symmetries in which the resonances appear, we have found that the dominant physics of relaxation of the target in the presence of an extra electron trapped in a shape resonance is captured by a "relaxed self-consistent field" procedure that includes only configurations involving symmetry- and spin-conserving single excitations of the target. This procedure and the other parameters of the calculation are described in Ref. [12].

The ${}^2\Pi_u$ resonance state splits into two nondegenerate states of symmetry 2A_1 and 2B_1 when the molecule is bent. Our earlier study [10] reported the behavior of the fixed-nuclei cross sections for the lower of these two states (2A_1) as a function of stretching and bending. For a bend angle of zero, the degenerate ${}^2\Pi_u$ state decreases in energy as the molecule is stretched, crossing the neutral ground state and becoming electronically bound at a CO distance of ~ 2.6 bohr. Upon bending, the width of the 2A_1 component of the resonance increases dramatically as it decreases in energy. For the 2B_1 (upper) state, however, the behavior with increasing bend angle is entirely different. Its width increases little as the molecule bends while maintaining the equilibrium CO distance, and it increases in energy. That behavior can be seen in the fixed-nuclei results in Fig. 1. These cross sections show the energy dependence of the resonance relative to the neutral ground state. The total electronic energy is the resonance energy plus the CO₂ ground-state energy. The absolute energy of the 2B_1 state rises as a function of increasing bend angle although it is seen to decrease slightly relative to the elastic threshold.

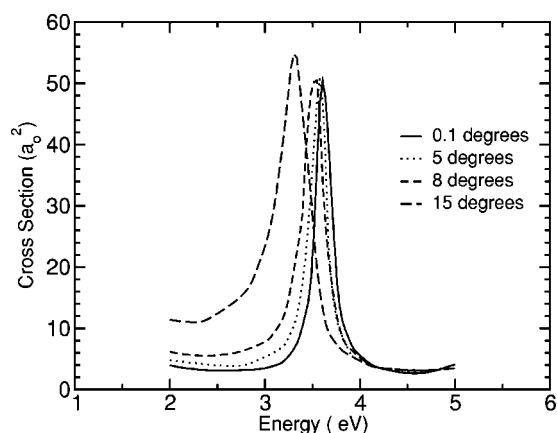


FIG. 1. $e^- + \text{CO}_2$ fixed-nuclei integrated cross section, in units of a_0^2 , in 2B_1 symmetry showing bend-angle dependence at equilibrium C—O bond distance.

It is well known [17,18] that the 2A_1 state of CO_2^- is a stable negative ion, i.e., electronically bound, when the molecule is either stretched or bent sufficiently. Stretching the molecule in linear geometry causes the width to decrease monotonically and the corresponding resonance parameters are straight forward to obtain by fitting the calculated eigenphase sums to a Breit-Wigner form with a smooth background. Calculating resonance parameters for large bending angles for the 2A_1 state, however, presents something of a problem, as we discussed earlier [10].

To understand why the width of the 2A_1 resonance state increases with increasing bend angle, one should first note that the symmetric-stretch motion with zero bend angle does not change the symmetry of the molecule, and hence does not significantly change the angular-momentum character of the resonance, whose lowest l component at equilibrium is p wave. Bending the molecule, however, breaks the degeneracy of the ${}^2\Pi_u$ resonance and mixes an s -wave component into the 2A_1 resonance. There is no angular-momentum barrier associated with an s wave, so it is not surprising that such an admixture causes the width, which is the inverse of the resonance lifetime, to increase. In 2B_1 symmetry, however, the s wave is not present and the resonance lifetime is relatively insensitive to bending. It is also important to note that upon bending CO_2 acquires a dipole moment.

At sufficiently large bending angles, CO_2^- becomes a bound state, and at first glance it is natural to expect that it is the 2A_1 resonance state that should become bound. However, the picture is likely to be more complicated than that. As we discussed earlier [10], the origin of the bound state of the anion seems to depend on the path of the nuclei. If the molecule is first stretched until the ${}^2\Pi_u$ resonance state becomes bound, and then bent to the equilibrium geometry of the CO_2^- bound anion, one concludes that it is the 2A_1 resonance state which becomes bound. However, the electron- CO_2 system also has a virtual state [19]. If one begins with that virtual state, and bends the molecule, it too can become bound. Then upon stretching the C—O bond distance one can arrive at the same equilibrium geometry for the CO_2^- bound anion state, but conclude that it is a different state.

In another study [20] we provided a model for how this puzzle about the topology of the resonant, virtual and bound states of CO_2^- might be resolved. That interpretation involves tracking the poles of the S matrix for a model for this system in the complex momentum plane and showing that there can be a conical intersection of the virtual and resonance states on a nonphysical Riemann sheet in the complex k plane of the S matrix. As a result, it is possible to show that transporting such a system around a closed loop in the configuration space of nuclear geometries can bring the system to a different state, and that two circuits of the loop are required to return the system to the same electronic phase with the accumulation of a Berry phase.

That complicated picture suggests that for large bending angles the simple two-component resonance picture of CO_2^- may break down. However, in the present calculations, we have considered dynamics (beginning with the ground vibrational state and ending with the molecule in the lowest Fermi dyad or triad states) that does not probe that region. In the calculations presented here, we have used the same complex potential surface for the 2A_1 resonance that we used in our earlier study [10] that included only one component of the resonance, and which is constructed from the fits of the fixed-nuclei cross sections to have a width that goes to zero continuously for bending angles where the anion is bound.

B. Parametrization of the complex resonance surfaces

From a series of fixed-nuclei scattering calculations in 2A_1 and 2B_1 symmetries we have constructed fits to both complex potential surfaces appropriate for dynamics calculations involving the symmetric stretch and bending modes of CO_2 . The real and imaginary parts of those surfaces, $E^{res} = E_{Real} - i\Gamma/2$, where Γ is the width, are shown in Fig. 2, and the different characters of the 2A_1 and 2B_1 states are immediately apparent. While the bending motion on the 2A_1 surface is down hill in energy toward the equilibrium configuration of CO_2^- , the bending motion on the 2B_1 is confined by a shallow potential well. Just as important for the dynamics is the dramatic difference in the behavior of the width. The increase in width of the 2A_1 with bending contrasts with the insensitivity of the width of 2B_1 to bending angle.

For the fits we define R_{CO} as the C—O bond length (in bohr) and the angle Θ as π minus the O—C—O bond angle in degrees. It is clear that for $\Theta = 0$ the two surfaces must be degenerate and have the same imaginary part as two components of the ${}^2\Pi_u$ resonance state. Therefore, our representations of the two surfaces contain terms depending only on R_{CO} added to terms that depend on both R_{CO} and Θ .

The real parts of the surfaces are described by

$$V_{A_1}(R_{CO}, \Theta) = M(R_{CO}) - F(R_{CO})(1.97676 \times 10^{-4} - 1.21529 \times 10^{-7} \Theta^2) \Theta^2 \quad (4)$$

for the 2A_1 state and

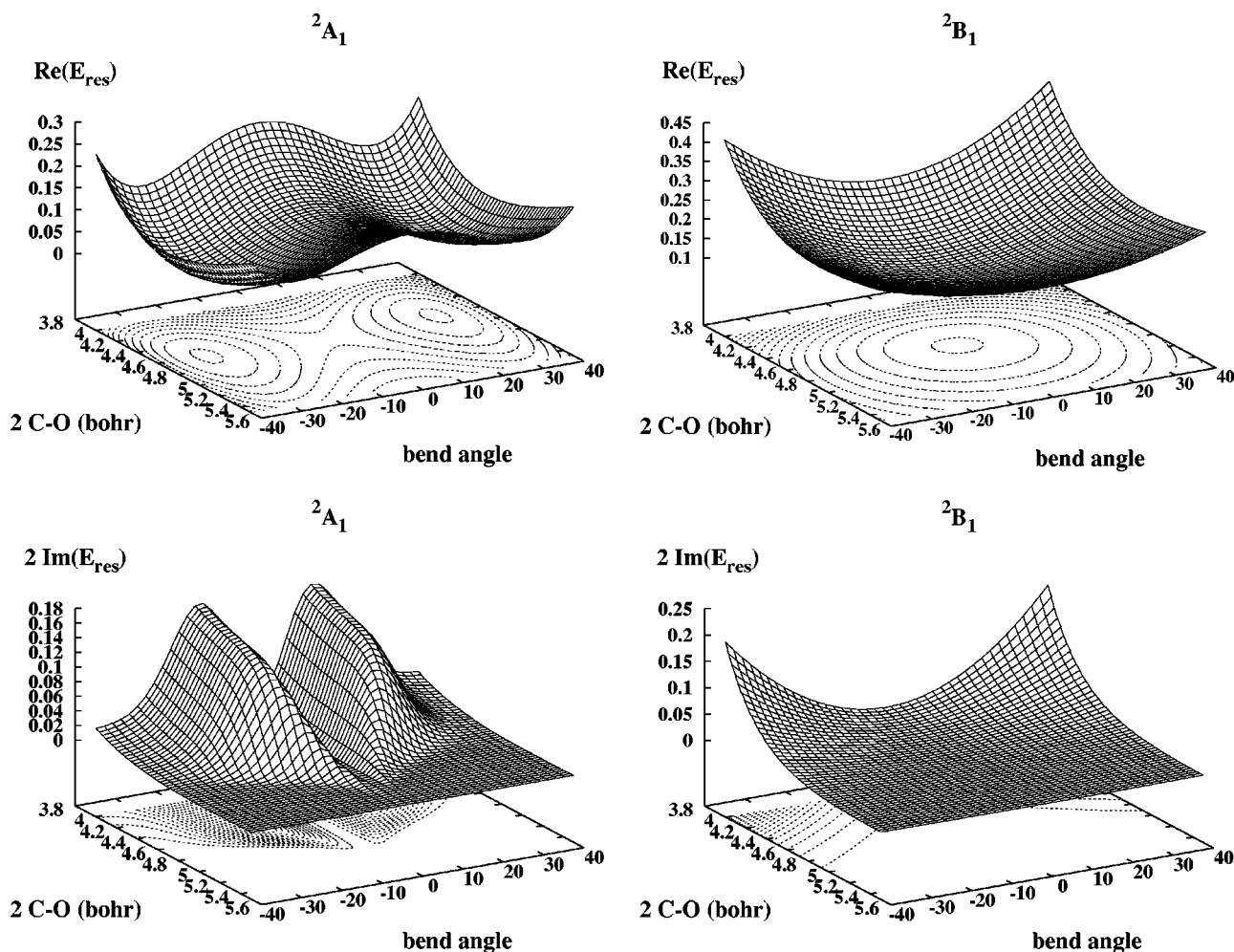


FIG. 2. Complex potential surfaces for both components of the resonance. Top row, real part of resonance energies; bottom row, widths. Energies are in hartrees and the bend angle, defined as π minus the O—C—O bond angle, is in degrees.

$$V_{B_1}(R_{CO}, \Theta) = M(R_{CO}) + (2.8988 \times 10^{-4} - 8.9627 \times 10^{-5} R_{CO}) \Theta^2 \quad (5)$$

for the 2B_1 component.

The widths are given by

$$\Gamma_{A_1}(R_{CO}, \Theta) = G(R_{CO}) + 0.002 \exp[-A(R_{CO}) \Theta^2] \Theta^2 \quad (6)$$

and

$$\Gamma_{B_1}(R_{CO}, \Theta) = G(R_{CO}) + \{45.559 \exp[-6.4623 R_{CO}]\} \Theta^2. \quad (7)$$

The functions $M(R_{CO})$ and $G(R_{CO})$, describing purely symmetric-stretching behavior, are

$$M(R_{CO}) = 0.117358 + 0.409035 \{1 - \exp[-1.370(R_{CO} - 2.33718)]\}^2 \quad (8)$$

and

$$G(R) = \begin{cases} 7.8608 - 11.9292 R_{CO} \\ + 6.8032 R_{CO}^2, & R_{CO} < 2.56 \\ -1.7282 R_{CO}^3 + 0.165008 R_{CO}^4 \\ 0, & R_{CO} \geq 2.56, \end{cases} \quad (9)$$

the latter function fixing the width at zero in the region where the anion is bound. The functions F and A involved in the terms that couple stretching and bending are defined as

$$F(R_{CO}) = \exp[-0.6(R_{CO} - 2.33)], \quad (10)$$

$$A(R_{CO}) = 0.005 + 2.5 \left[1 - \frac{1}{1 + \exp[20(R_{CO} - 2.7)]} \right]. \quad (11)$$

Equipped with these representations of the *ab initio* resonance parameters we have all the requirements to perform local complex potential or boomerang calculations for the resonant vibrational excitation cross sections. However, we must first formulate the local complex potential model for two resonances with the appropriate coupling.

III. THE BOOMERANG MODEL FOR COUPLED ELECTRON-SCATTERING RESONANCES IN POLYATOMIC MOLECULES

The local complex potential, or boomerang [6], model is derived using Feshbach partitioning [21] to first separate resonant and nonresonant scattering and then applying a number of simplifying assumptions to obtain an effective Schrödinger equation for nuclear motion in the body-fixed frame. The key approximations are the assumption that the energetically open vibrational states of the target form a complete set, at least over the region of space spanned by the initial target vibrational level, and that the electronic coupling element between the resonance state and the background continuum be approximately independent of the ejected electron energy. These approximations require that the incident electron energy be much larger than the target vibrational energy spacing. The limits of validity of these approximations are well understood [22], and have been tested in a few calculations using more rigorous nonlocal formulations [23–25]. The boomerang model will obviously break down near the thresholds for vibrational excitation, and we have not attempted to apply it near the elastic threshold where other effects are expected to be operative. For a diatomic molecule there is only a single vibrational degree of freedom, and in the case of an isolated resonance the working expressions of the theory are quite simple. The equation that determines the nuclear dynamics is

$$[E - K_R - E_r(R) + i\Gamma(R)/2]\xi_\nu(R) = \phi_\nu(R). \quad (12)$$

In Eq. (12), the negative-ion energy surface is characterized by a real part $E_r(R)$ and an imaginary part $-i\Gamma(R)/2$. The nuclear kinetic-energy operator is denoted by K_R , and the “entry amplitude,” ϕ_ν , is defined as

$$\phi_\nu(R) = [\Gamma(R)/2\pi]^{1/2} \chi_\nu(R), \quad (13)$$

where χ_ν is the initial vibrational wave function of neutral target.

The resonant T matrix for vibrational excitation is obtained by projecting the solution of Eq. (12) onto the “exit amplitude,” $\phi_{\nu'}$:

$$T_{\nu\nu'}(E) = \langle \phi_{\nu'} | \xi_\nu \rangle. \quad (14)$$

Combining Eqs. (12) and (14) allows us to write $T_{\nu\nu'}(E)$ as the matrix element of a nuclear Green’s function between entry and exit amplitudes,

$$T_{\nu\nu'}(E) = \left\langle \phi_{\nu'} \left| \frac{1}{E - K_R - E_r(R) + i\Gamma(R)/2} \right| \phi_\nu \right\rangle. \quad (15)$$

Because the majority of applications of this theory have been to diatomics, it has become conventional to write the working equations of the local complex potential theory in this manner, and avoid the more rigorous discussion, in which the entry and exit amplitudes have an implicit dependence on the angles specifying the orientation of molecular frame with respect to the incident momentum of the electron in the laboratory frame. The integral cross sections are then

proportional to the modulus squared of the amplitude in Eq. (15). However in the polyatomic case there are some subtleties, particularly, with respect to constructing the differential *and* integral cross sections from the T matrices of this theory, that are obscured by these formulations. Estrada *et al.* [15] have discussed this point with considerable care in the context of coupled resonances in polyatomic systems.

Our formulation follows theirs in most respects and specializes it to the case at hand, in which the symmetries of the components of the CO₂⁻ resonance negate the assumptions they used to formulate the model problem with which they explored these questions. The goal is to obtain working equations that have the form of Eqs. (12)–(15) in the body-fixed frame, but also obtain the correct connection of those amplitudes to the integral and differential cross sections.

A. The case of two-coupled overlapping resonances

We take up the formulation at the point of expressing the nuclear wave equation, after some of the usual assumptions of the local complex potential theory have been made [15]. Labeling the two resonances “1” and “2” we first define a vector of nuclear wave functions in a notation that preserves the dependence on the direction of the incoming electron, whose incident momentum we denote by \mathbf{k} ,

$$\vec{\xi}_{\mathbf{k}\nu}(R) = \begin{pmatrix} \xi_{1\mathbf{k}\nu}(R) \\ \xi_{2\mathbf{k}\nu}(R) \end{pmatrix}, \quad (16)$$

These are the components of the nuclear wave function on the two resonance surfaces. We similarly define the driving vector of the nuclear wave equation according to

$$\vec{X}_{\mathbf{k}\nu}(R) = \begin{pmatrix} X_{1\mathbf{k}\nu}(R) \\ X_{2\mathbf{k}\nu}(R) \end{pmatrix}. \quad (17)$$

Later we will make an assumption characteristic of the boomerang model below in which the dependence of $\vec{X}_{\mathbf{k}\nu}(R)$ on the wave vector of the incident electron, \mathbf{k} , will be made explicit. Here and elsewhere, we use R to denote collectively the nuclear coordinates.

The nuclear wave equation is then a vector equation, with a 2×2 Hamiltonian matrix that acts on the components of the nuclear wave function on each of the two coupled resonance surfaces,

$$(E - H)\vec{\xi}_{\mathbf{k}\nu}(R) = \vec{X}_{\mathbf{k}\nu}(R). \quad (18)$$

The Hamiltonian for this equation can be written in the form

$$H = \begin{bmatrix} K_R + V_1(R) & W_{1,2}(R) + U_{1,2}(R) \\ W_{2,1}(R) + U_{2,1}(R) & K_R + V_2(R) \end{bmatrix}, \quad (19)$$

in which K_R denotes the nuclear kinetic energy; V_i , $i = 1, 2$, denotes the complex potential surface of each of the two resonances; and $W_{i,j}(R)$ and $U_{i,j}(R)$ denote two possible types of couplings between the resonance states.

Estrada *et al.* [15] make an important observation about the question of the vibronic couplings. One kind of coupling,

which we call here $W_{i,j}(R)$, is a coupling through the continuum to which the resonances can decay [26,27]. In essence, the electron can escape from one resonance state and be recaptured into the other. However, in the present case the two resonances have different molecular symmetries, and therefore are coupled to continua of different symmetries. This mechanism, therefore, cannot couple the 2A_1 and 2B_1 resonances of CO_2 . The other coupling, denoted here by $U_{i,j}$, is nonadiabatic coupling originating in the nuclear kinetic energy and the breakdown of the Born-Oppenheimer approximation for nearly degenerate states. The components of the ${}^2\Pi_u$ resonance in CO_2^- are coupled by a classic form of nonadiabatic coupling familiar from molecular spectroscopy, called the Renner-Teller effect, in which the angular momentum associated with the degenerate bending modes of the molecule couples to the electronic angular momentum of the resonance state. However, before we discuss the explicit form of the coupling, we must confront the question of how to extract the cross sections from the solutions of the two-dimensional nuclear wave equation.

We can solve Eq. (18) formally,

$$\vec{\xi}_{\mathbf{k}\nu}(R) = (E - H + i\eta)^{-1} \vec{X}_{\mathbf{k}\nu}(R), \quad (20)$$

and use the result in an expression analogous to Eq. (14) to obtain a matrix equation for the T matrix like that in Eq. (15),

$$T_{\mathbf{k}'\nu',\mathbf{k},\nu}(E) = \int \int \vec{X}_{\mathbf{k}'\nu'}(R)^\dagger (E - H + i\eta)^{-1} \times \vec{X}_{\mathbf{k}\nu}(R') dR' dR. \quad (21)$$

There are four contributions to this amplitude that we can denote by T_{ij} ,

$$T_{ij} = \int \int X_{i\mathbf{k}'\nu'}(R)^\dagger [(E - H + i\eta)^{-1}]_{ij} X_{j\mathbf{k}\nu}(R') dR' dR, \quad (22)$$

so that

$$T_{\mathbf{k}'\nu',\mathbf{k},\nu}(E) = \sum_{i,j=1}^2 T_{ij}. \quad (23)$$

Each term in this sum can have a different angular dependence that arises from the entry and exit amplitudes $X_{i\mathbf{k}\nu}$.

To get the contributions from which the integral and differential cross sections are to be constructed we need to invoke the further approximation, intrinsic to the boomerang model and familiar from the original literature [6,7,22] on the subject, that these amplitudes factor because the entry and exit amplitudes factor according to the formula

$$X_{i\mathbf{k}\nu}(R) = \left(\frac{\Gamma_i(R)}{2\pi} \right)^{1/2} \chi_\nu(R) Y_{l_i, m_i}(\mathbf{k}), \quad (24)$$

where $\chi_\nu(R)$ is a vibrational state of the neutral molecule, and $Y_{l_i, m_i}(\mathbf{k})$ is an angular function with (l_i, m_i) denoting the angular-momentum quantum numbers of the i th initial state.

The axis of quantization for the angular functions is in the laboratory-fixed frame and will be chosen below to coincide with the direction of the incident electron momentum. Depending on the symmetries of the resonances, the angular function can be a linear combination of spherical harmonics of the same l but different m . We will use the notation Y_i below to denote such functions.

Under the usual assumptions of effective degeneracy of molecular rotational levels, the differential cross section is related to this T matrix by an average over molecular orientations,

$$\frac{d\sigma_{\mathbf{k}'\nu',\mathbf{k},\nu}(E)}{d\Omega} = \frac{(2\pi)^4}{k^2} \overline{|T_{\mathbf{k}'\nu',\mathbf{k},\nu}(E)|^2}, \quad (25)$$

where the average over the orientations of the molecule is denoted by the bar. The integral cross section for vibrational excitation is then given by

$$\sigma_{\mathbf{k}'\nu',\mathbf{k},\nu}(E) = \frac{(2\pi)^4}{k^2} \int \overline{|T_{\mathbf{k}'\nu',\mathbf{k},\nu}(E)|^2} d\Omega. \quad (26)$$

We now have the task of explicitly evaluating, for example, the expression for the differential cross section

$$\frac{d\sigma_{\mathbf{k}'\nu',\mathbf{k},\nu}(E)}{d\Omega} = \frac{(2\pi)^4}{k^2} \overline{|T_{11} + T_{12} + T_{21} + T_{22}|^2}, \quad (27)$$

and writing the result in terms of amplitudes that arise from solving the equation analogous to Eq. (20), in which the entry and exit amplitudes have the form $(\Gamma_i(R)/2\pi)^{1/2} \chi_\nu(R)$, i.e., do not contain a dependence on the direction of the momentum of the incident or exiting electron. Then we will have reduced the nuclear wave equation to a form that can be solved entirely in the molecule-fixed frame of reference. The connection with the laboratory frame is made through the average over molecular orientations.

With the factorization in Eq. (24) the contributions to the T matrix can be written in the form

$$T_{ij} = Y_i(\mathbf{k})^* t_{ij} Y_j(\mathbf{k}). \quad (28)$$

The amplitudes t_{ij} originate from the effective nuclear wave equation, now expressed entirely in the body-fixed frame,

$$\vec{\xi}_\nu(R) = (E - H + i\eta)^{-1} \vec{X}_\nu(R), \quad (29)$$

and are defined according to

$$t_{ij} = \int \int X_{i\nu'}(R)^\dagger [(E - H + i\eta)^{-1}]_{ij} X_{j\nu}(R') dR' dR \quad (30)$$

with entry and exit amplitudes defined by

$$X_{i\nu}(R) = \left(\frac{\Gamma_i(R)}{2\pi} \right)^{1/2} \chi_\nu(R). \quad (31)$$

Equations (29)–(31) are the working expressions of the local complex potential theory for coupled resonances in a polyatomic system. They have no reference to the direction of the incident and exiting momentum of the scattered electron, as one expects from the familiar boomerang theory for isolated resonances. The explicit form of the Hamiltonian, H , for the case of Renner-Teller coupling will be discussed in the following sections. At this point, however, the question is how to evaluate the cross sections once we have solved these equations.

Inserting Eqs. (28) and (23) into the equations for the cross sections, Eqs. (25) and (26), provides the starting point for deriving the explicit connections of the t_{ij} amplitudes to those cross sections. We will show in the following section that the integral cross section takes a simple form in this case, somewhat different from the case considered by Estrada *et al.* [15]:

$$\sigma_{\nu',\nu}(E) = \frac{4\pi^3}{k^2} (|t_{11}|^2 + |t_{22}|^2 + |t_{12}|^2 + |t_{21}|^2) = \frac{4\pi^3}{k^2} \text{tr}(\mathbf{t}^\dagger \mathbf{t}). \quad (32)$$

To derive this equation, and the corresponding one for the differential cross sections, we must explicitly perform the average over molecular orientations in Eqs. (25) and (26) for the particular case of the 2A_1 and 2B_1 symmetries arising from the ${}^2\Pi_u$ resonance, and that is the task to which we now turn.

B. Angular dependence

The dominant component of the ${}^2\Pi_u$ resonance has angular momentum $l=1$ with $m=\pm 1$. So in Eq. (28) one could associate the two components of the resonance, $i=1,2$ with $m=\pm 1$. However, upon bending, the components of ${}^2\Pi_u$ transform with the molecular symmetries 2A_1 and 2B_1 , which do not map onto single values of m . Since we have used the electronic basis that transforms with molecular symmetries in the formulation of the nuclear wave equation, we must therefore use the combinations of the usual spherical harmonics, Y_{lm} that transform with x and y . Those “real spherical harmonics” are defined by

$$\begin{pmatrix} Y_x \\ Y_y \end{pmatrix} = \begin{pmatrix} 1/\sqrt{2} & -1/\sqrt{2} \\ i/\sqrt{2} & i/\sqrt{2} \end{pmatrix} \begin{pmatrix} Y_{1,-1}^{mol} \\ Y_{1,1}^{mol} \end{pmatrix} \equiv \mathbf{M} \begin{pmatrix} Y_{1,-1}^{mol} \\ Y_{1,1}^{mol} \end{pmatrix}, \quad (33)$$

where we have emphasized the fact that they are specified in the molecule-fixed frame.

These are the angular functions that appear in Eq. (28), with $i=1$ corresponding to Y_x and $i=2$ corresponding to Y_y , and our task in this section is to evaluate the average over orientations of the molecule-fixed frame in Eq. (27) using these definitions. To simplify angular-momentum algebra of the average over molecular orientations, we first define a set of amplitudes, τ_{m_i, m_j} , that refer to the usual spherical harmonics with $m=\pm 1$,

$$\boldsymbol{\tau} = \mathbf{M}^\dagger \mathbf{t} \mathbf{M}. \quad (34)$$

Expressed in terms of these amplitudes, Eq. (23) now reads

$$T_{\mathbf{k}'\nu',\mathbf{k}\nu}(E) = \sum_{m_i, m_f} Y_{1, m_f}^{mol*}(\mathbf{k}') \tau_{m_f, m_i} Y_{1, m_i}^{mol}(\mathbf{k}). \quad (35)$$

The average over molecular orientations in Eq. (27) can be written in terms of the Euler angles relating the molecular and laboratory frames as

$$\overline{|T_{\mathbf{k}'\nu',\mathbf{k}\nu}(E)|^2} = \frac{1}{8\pi^2} \int |T_{\mathbf{k}'\nu',\mathbf{k}\nu}(E)|^2 d\omega, \quad (36)$$

where $d\omega = \sin\beta d\alpha d\beta d\gamma$. The explicit dependence on these Euler angles of the molecule-fixed spherical harmonics, $Y_{1,m}^{mol}(\mathbf{k})$, is given by the familiar relation [28],

$$Y_{1,m}^{mol}(\mathbf{k}) = \sum_{\mu} Y_{1,\mu}^{lab}(\mathbf{k}) D_{\mu,m}^1(\alpha, \beta, \gamma), \quad (37)$$

where $D_{\mu,m}^1(\alpha, \beta, \gamma)$ is a Wigner rotation matrix. With these substitutions, Eq. (35) now reads

$$\begin{aligned} T_{\mathbf{k}'\nu',\mathbf{k}\nu}(E) &= \sum_{m_i, m_f, \mu, \mu'} Y_{1,\mu}^{lab*}(\mathbf{k}') D_{\mu, m_f}^{1*}(\alpha, \beta, \gamma) \tau_{m_f, m_i} \\ &\quad \times Y_{1,\mu'}^{lab}(\mathbf{k}) D_{\mu', m_i}^1(\alpha, \beta, \gamma). \end{aligned} \quad (38)$$

We can simplify the integral over Euler angles in Eq. (36) considerably by choosing the z axis of the laboratory frame to coincide with the direction of the incident momentum \mathbf{k} . Then we can use the identity (because only $\mu=0$ contributes)

$$\sum_{\mu} Y_{1,\mu}(\mathbf{k}) D_{\mu,m}^1(\alpha, \beta, \gamma) = Y_{1,m}(\beta, \gamma) \quad (39)$$

to rewrite Eq. (36) as

$$\begin{aligned} &\frac{1}{8\pi^2} \int |T_{\mathbf{k}'\nu',\mathbf{k}\nu}(E)|^2 d\omega \\ &= \sum_{m_i, m_f, n_i, n_f} \tau_{n_f, n_i}^* \tau_{m_f, m_i} \sum_{\mu, \mu'} Y_{1,\mu'}(\mathbf{k}') Y_{1,\mu}^*(\mathbf{k}') \\ &\quad \times \frac{1}{8\pi^2} \int D_{\mu', n_f}^1(\alpha, \beta, \gamma) D_{\mu, m_f}^{1*}(\alpha, \beta, \gamma) Y_{1, n_i}^*(\beta, \gamma) \\ &\quad \times Y_{1, m_i}(\beta, \gamma) d\omega. \end{aligned} \quad (40)$$

We are still left with integrals of the products of four functions of the Euler angles, but using the relation

$$Y_{l,m}(\beta, \gamma) = \sqrt{\frac{2l+1}{4\pi}} D_{0,m}^l(\alpha, \beta, \gamma), \quad (41)$$

we can write those as products of four Wigner rotation matrices. Then we can use the product rule

$$D_{m'_1, m_1}^{j_1}(\omega) D_{m'_2, m_2}^{j_2}(\omega) = \sum_{m, m', j} (2j+1) D_{m', m}^{j*}(\omega) \times \begin{pmatrix} j_1 & j_2 & j \\ m_1 & m_2 & m \end{pmatrix} \begin{pmatrix} j_1 & j_2 & j \\ m'_1 & m'_2 & m' \end{pmatrix} \quad (42)$$

and the formula for the integral of three rotation matrices

$$\frac{1}{8\pi^2} \int D_{m'_1, m_1}^{j_1}(\alpha, \beta, \gamma) D_{m'_2, m_2}^{j_2}(\alpha, \beta, \gamma) D_{m'_3, m_3}^{j_3}(\alpha, \beta, \gamma) d\omega = \begin{pmatrix} j_1 & j_2 & j_3 \\ m_1 & m_2 & m_3 \end{pmatrix} \begin{pmatrix} j_1 & j_2 & j_3 \\ m'_1 & m'_2 & m'_3 \end{pmatrix} \quad (43)$$

to perform all the integrals in Eq. (40). After some algebra we obtain the result for the average over molecular orientations in terms of spherical harmonics of angles specifying the direction of the ejected electron and Wigner three- j symbols

$$\begin{aligned} & \frac{1}{8\pi^2} \int |T_{\mathbf{k}'\nu', \mathbf{k}\nu}(E)|^2 d\omega \\ &= \sum_{m_i, m_f, n_i, n_f} \tau_{n_f, n_i}^* \tau_{m_f, m_i} \sum_{j, \mu} Y_{1, \mu}(\mathbf{k}') Y_{1, \mu}^*(\mathbf{k}) \\ & \times \begin{pmatrix} 1 & 1 & j \\ \mu & 0 & -\mu \end{pmatrix}^2 \begin{pmatrix} 1 & 1 & j \\ m_f & n_i & m \end{pmatrix} \\ & \times \begin{pmatrix} 1 & 1 & j \\ n_f & m_i & m \end{pmatrix} \frac{3}{4\pi} (2j+1). \end{aligned} \quad (44)$$

We can now use Eq. (44) in Eq. (25) and evaluate the spherical harmonics and three- j symbols explicitly to obtain the final result for the differential cross section,

$$\begin{aligned} \frac{d\sigma_{\nu', \nu}}{d\Omega}(E) &= \frac{3\pi^2}{20k^2} \{ [7 + \cos(2\theta)] (|\tau_{1,1}|^2 + |\tau_{-1,-1}|^2 \\ & + |\tau_{1,-1}|^2 + |\tau_{-1,1}|^2) + [1 \\ & + 3 \cos(2\theta)] 4 \operatorname{Re}(\tau_{1,1}^* \tau_{-1,-1}) \}. \end{aligned} \quad (45)$$

This expression differs in a key way from Dube and Herzenberg's [7] result for an isolated resonance in the case of a diatomic target. For an isolated resonance the factorization of the T matrix in our Eq. (28) leads to only a single term in Eq. (27). The result is that the differential cross section in this theory for an isolated resonance takes the form

$$\frac{d\sigma_{\nu', \nu}}{d\Omega}(E) = g(\theta) \sigma_{\nu', \nu}(E) \quad (46)$$

and consists of an energy-independent angular factor, $g(\theta)$, multiplied by the energy-dependent integral cross section.

That is not the case for multiple resonances, and an interference term appears in Eq. (45) due to the coupling between the resonances. This fact was pointed out by Estrada *et al.* [15], but the case they considered involved resonances having different parities under inversion, and their final result does not involve all four contributions for the T matrix in Eq. (27).

It is interesting to note that Eq. (45) can be specialized to the case of a doubly degenerate ${}^2\Pi_u$ resonance by setting $\tau_{1,1} = \tau_{-1,-1}$ and setting the coupling to zero, $\tau_{1,-1} = \tau_{-1,1}$. The result is

$$\frac{d\sigma}{d\Omega} = \frac{3\pi^2}{10k^2} |\tau|^2 [9 + 7 \cos(2\theta)]. \quad (47)$$

This result has the form of Eq. (46) and can also be gotten by evaluating Eqs. (2.65) and (2.66) of Dube and Herzenberg's [7] original analysis for diatomics with $l_{min} = 1$.

The integral cross section in Eq. (26) is found from Eq. (45) by integrating over the directions of the exiting electron, and takes the simple form

$$\begin{aligned} \sigma_{\nu', \nu}(E) &= \frac{4\pi^3}{k^2} (|\tau_{1,1}|^2 + |\tau_{-1,-1}|^2 + |\tau_{1,-1}|^2 + |\tau_{-1,1}|^2) \\ &= \frac{4\pi^3}{k^2} \operatorname{tr}(\boldsymbol{\tau}^\dagger \boldsymbol{\tau}) \\ &= \frac{4\pi^3}{k^2} \operatorname{tr}(\boldsymbol{t}^\dagger \boldsymbol{t}), \end{aligned} \quad (48)$$

where the last equality arises because the body-fixed $\boldsymbol{\tau}$ and \boldsymbol{t} amplitudes are related by the unitary transformation defined explicitly in Eqs. (33) and (34). The amplitudes, t_{ij} , refer to the four possibilities for entering and exiting, respectively, in the 2A_1 and 2B_1 resonance states. The result expressed in Eqs. (32) and (48) is that the integral cross section is given by an incoherent sum of those four contributions to the T matrix.

With the local complex potential theory formulated for our case of two-coupled resonances that arise from the ${}^2\Pi_u$ resonance in CO_2 , we are ready to turn to the question of the nonadiabatic coupling between them.

IV. RENNER-TELLER COUPLING IN ELECTRON-SCATTERING RESONANCES

For linear triatomic molecules, the nonadiabatic coupling between components of Π , Δ , etc., electronic states whose degeneracy is lifted upon bending is a phenomenon that is well understood in molecular spectroscopy. It was first predicted by Renner [29] in 1934, and has been observed and analyzed quantitatively in a number of physical systems. These well-understood examples involve states of linear molecules that are electronically bound. Our discussion of

this effect in the context of resonance states, whose finite lifetimes give rise to a complex potential surface for each component of the pair of Renner-Teller coupled states, follows the treatments for bound states given in the extensive reviews of Brown and Jorgensen [30] and Jungen and Merer [31]. Our goal here is to specialize the classic treatment of this effect to the case of the ${}^2\Pi_u$ state of CO₂⁻ and express the result in terms of diabatic states that correlate properly with the 2A_1 and 2B_1 resonance states.

We begin by focusing on the nuclear kinetic-energy operator in the Schrödinger equation for a linear molecule,

$$(\mathcal{H}-E)\Psi=0 \quad (49)$$

with

$$\mathcal{H}=K_n+H_{el}, \quad (50)$$

where K_n denotes the nuclear kinetic-energy operator. We will formulate the coupling between the 2A_1 and 2B_1 states using normal coordinates for the nuclear motion. We denote the normal coordinate for symmetric stretch by s_1 and those of the degenerate bending modes by s_{2a} and s_{2b} . Neglecting the end-over-end rotations of the molecule we can write the kinetic energy for nuclear motion in the form

$$K_n=-\frac{1}{2\mu_1}\frac{\partial^2}{\partial s_1^2}-\frac{1}{2\mu_2}\left(\frac{\partial^2}{\partial s_{2a}^2}+\frac{\partial^2}{\partial s_{2b}^2}\right). \quad (51)$$

In Eq. (51) the reduced masses are given in terms of the carbon and oxygen atomic masses by

$$\mu_1=M_o/2 \quad (52)$$

and

$$\mu_2=M_c\left(1+\frac{M_c}{2M_o}\right). \quad (53)$$

The potentials for bending must be functions of only $\sqrt{s_{2a}^2+s_{2b}^2}$, because they cannot depend on orientation of the plane in which the molecule bends. So we can transform to the polar coordinates ρ and α

$$\rho=\sqrt{s_{2a}^2+s_{2b}^2}, \quad (54)$$

$$\alpha=\tan^{-1}(s_{2b}/s_{2a}). \quad (55)$$

Taking out a factor of $\rho^{1/2}$,

$$\Psi=\Phi/\rho^{1/2}, \quad (56)$$

we find

$$K_n=-\frac{1}{2\mu_1}\frac{\partial^2}{\partial s_1^2}+\frac{1}{\mu_2}\times\left(-\frac{1}{2}\frac{\partial^2}{\partial \rho^2}-\frac{1}{8\rho^2}-\frac{1}{2\rho^2}\frac{\partial^2}{\partial \alpha^2}\right). \quad (57)$$

We can identify the operator $-\partial^2/\partial \alpha^2$ with the square of the component of rotational angular momentum about the figure axis, N_z , and rewrite this equation as

$$K_n=-\frac{1}{2\mu_1}\frac{\partial^2}{\partial s_1^2}-\frac{1}{2\mu_2}\frac{\partial^2}{\partial \rho^2}+\frac{1}{2\mu_2\rho^2}\left(N_z^2-\frac{1}{4}\right). \quad (58)$$

The Renner-Teller analysis now replaces N_z by the difference between the z components of the total angular momentum J_z and the electronic angular momentum L_z to obtain

$$K_n=-\frac{1}{2\mu_1}\frac{\partial^2}{\partial s_1^2}-\frac{1}{2\mu_2}\frac{\partial^2}{\partial \rho^2}+\frac{1}{2\mu_2\rho^2}\left((J_z-L_z)^2-\frac{1}{4}\right). \quad (59)$$

With the nuclear kinetic energy in this form, we can proceed to write the total wave function as a linear combination of products of the two electronic states and nuclear wave functions associated with each,

$$\Phi(r,s_1,\rho,\chi)=\phi_+(r,s_1,\rho)\eta_+(s_1,\rho,\chi)+\phi_-(r,s_1,\rho)\eta_-(s_1,\rho,\chi), \quad (60)$$

in which r denotes collectively the electronic coordinates and χ denotes the angle defining the orientation of the x - z plane for electrons and nuclei. The electronic wave functions are defined such that the zeroth-order component is either the x or the y component of the Π state (suppressing the symmetric stretch coordinate for the moment),

$$\phi_+(r,\rho)=\phi_{\Pi_x}(r)+\phi'_+(r)\rho+\dots, \quad (61)$$

$$\phi_-(r,\rho)=\phi_{\Pi_y}(r)+\phi'_-(r)\rho+\dots. \quad (62)$$

Keeping just the leading terms and using

$$L_z\phi_{\Pi_y}(r)=-i\Lambda\phi_{\Pi_x}(r), \quad (63)$$

$$L_z\phi_{\Pi_x}(r)=i\Lambda\phi_{\Pi_y}(r), \quad (64)$$

$$L_z^2\phi_{\Pi_{x,y}}(r)=\Lambda^2\phi_{\Pi_{x,y}}(r), \quad (65)$$

where $\Lambda=1$ is the magnitude of the z component of the electronic angular momentum for a ${}^2\Pi_u$ state, we get the Renner-Teller equation for nuclear motion by operating with the total Hamiltonian in Eq. (50) on Φ in Eq. (60),

$$\begin{pmatrix} -\frac{1}{2\mu_1} \frac{\partial^2}{\partial s_1^2} - \frac{1}{2\mu_2} \frac{\partial^2}{\partial \rho^2} + \frac{1}{2\mu_2 \rho^2} \left(-\frac{\partial^2}{\partial \chi^2} + \Lambda^2 - \frac{1}{4} \right) + V_{\Pi_x} & i/(\mu_2 \rho^2) \Lambda \left(-i \frac{\partial}{\partial \chi} \right) \\ -i/(\mu_2 \rho^2) \Lambda \left(-i \frac{\partial}{\partial \chi} \right) & -\frac{1}{2\mu_1} \frac{\partial^2}{\partial s_1^2} - \frac{1}{2\mu_2} \frac{\partial^2}{\partial \rho^2} + \frac{1}{2\mu_2 \rho^2} \left(-\frac{\partial^2}{\partial \chi^2} + \Lambda^2 - \frac{1}{4} \right) + V_{\Pi_y} \end{pmatrix} \times \begin{pmatrix} \eta_+(s_1, \rho, \chi) \\ \eta_-(s_1, \rho, \chi) \end{pmatrix} = E \begin{pmatrix} \eta_+(s_1, \rho, \chi) \\ \eta_-(s_1, \rho, \chi) \end{pmatrix}. \quad (66)$$

In Eq. (66) the electronic potential surfaces of the two resonances are denoted by $V_{\Pi_{x,y}} = V_{\Pi_{x,y}}(s_1, \rho)$ and depend only on the internal vibrational coordinates of the molecule.

Now, following Ref. [30], we can associate the operator $J_z = -i\partial/\partial\chi$ with its eigenvalue, K , by assuming the factorized form for the wave function,

$$\begin{pmatrix} \eta_+(s_1, \rho, \chi) \\ \eta_-(s_1, \rho, \chi) \end{pmatrix} = \begin{pmatrix} R_{K,+}(s_1, \rho) \\ R_{K,-}(s_1, \rho) \end{pmatrix} e^{iK\chi}. \quad (67)$$

This replacement brings us to the final form of the nuclear Schrödinger equation for the case at hand,

$$\begin{pmatrix} -\frac{1}{2\mu_1} \frac{\partial^2}{\partial s_1^2} - \frac{1}{2\mu_2} \frac{\partial^2}{\partial \rho^2} + \frac{1}{2\mu_2 \rho^2} \left(K^2 + \Lambda^2 - \frac{1}{4} \right) + V_{\Pi_x} & i\Lambda K/(\mu_2 \rho^2) \\ -i\Lambda K/(\mu_2 \rho^2) & -\frac{1}{2\mu_1} \frac{\partial^2}{\partial s_1^2} - \frac{1}{2\mu_2} \frac{\partial^2}{\partial \rho^2} + \frac{1}{2\mu_2 \rho^2} \left(K^2 + \Lambda^2 - \frac{1}{4} \right) + V_{\Pi_y} \end{pmatrix} \times \begin{pmatrix} R_{K,+}(s_1, \rho) \\ R_{K,-}(s_1, \rho) \end{pmatrix} = E \begin{pmatrix} R_{K,+}(s_1, \rho) \\ R_{K,-}(s_1, \rho) \end{pmatrix}. \quad (68)$$

From Eq. (68) we can read off the Hamiltonian for the nuclear wave equation of the boomerang model in Eq. (29),

$$H = \begin{pmatrix} -\frac{1}{2\mu_1} \frac{\partial^2}{\partial s_1^2} - \frac{1}{2\mu_2} \frac{\partial^2}{\partial \rho^2} + \frac{1}{2\mu_2 \rho^2} \left(K^2 + \Lambda^2 - \frac{1}{4} \right) + V_{A_1} & i\Lambda K/(\mu_2 \rho^2) \\ -i\Lambda K/(\mu_2 \rho^2) & -\frac{1}{2\mu_1} \frac{\partial^2}{\partial s_1^2} - \frac{1}{2\mu_2} \frac{\partial^2}{\partial \rho^2} + \frac{1}{2\mu_2 \rho^2} \left(K^2 + \Lambda^2 - \frac{1}{4} \right) + V_{B_1} \end{pmatrix}, \quad (69)$$

which we now have in the adiabatic representation that is directly connected to the molecular symmetries of the resonance states in our *ab initio* electron-scattering calculations. The complex potential surfaces of the two resonance states are denoted by V_{A_1} and V_{B_1} , and are functions of s_1 and ρ . Equation (69) defines the Hamiltonian that we will use in our local complex potential calculations to treat the motion of the nuclei on the coupled resonance surfaces.

We are interested in electron collisions with CO_2 in its ground electronic ($^1\Sigma_g$) and vibrational state. The projection of rotational and electronic angular momentum on the molecular axis in this initial neutral state is therefore zero. After the resonant capture of the electron into the temporary anion state, the projection of the electronic angular momentum on this axis, which is also the projection of the total angular

momentum because of the initial state of the target, is ± 1 . We therefore set $K=1$ and $\Lambda=1$ in Eq. (69) that defines the Hamiltonian for nuclear motion in the negative ion. However, for the initial and final vibrational states that appear in the entry and exit amplitudes in Eq. (31), we are dealing with vibrational levels of the neutral target in its ground electronic state, which has $^1\Sigma_g$ symmetry, and therefore corresponds to $\Lambda=0$. The vibrational levels which we will be considering as initial and final states are the ground vibrational state and the first Fermi dyad and triad, respectively, all of which have zero angular momentum about the figure axis, and therefore correspond to $K=0$. To compute these vibrational states, we use the same normal coordinates in a one-channel version of Eq. (69) with $K=0$ and $\Lambda=0$ and employ the (real) SCF potential surface we calculated for the ground state,

$$H = -\frac{1}{2\mu_1} \frac{\partial^2}{\partial s_1^2} - \frac{1}{2\mu_2} \frac{\partial^2}{\partial \rho^2} - \frac{1}{8\mu_2 \rho^2} + V_{SCF(1\Sigma_g)}. \quad (70)$$

We reiterate that the reason that the total angular momentum in the Renner-Teller Hamiltonian for nuclear motion in the resonance state is different from that in the initial state of the system is that the incident (and exiting) electron carry non-zero orbital angular momentum.

Now we can turn to the problem of the numerical solution of the equations for nuclear motion in the boomerang model given in Eqs. (29)–(31) using the Hamiltonian in Eq. (69).

V. NUMERICAL SOLUTION OF THE EQUATIONS OF THE LOCAL COMPLEX POTENTIAL MODEL FOR COUPLED RESONANCE STATES

The first step in our solution of Eqs. (29)–(31) is to recast them in a time-dependent form. The time-dependent formulation of the boomerang model, first described by McCurdy and Turner [13], starts from the observation that Green's function in Eq. (30) can be written as the Fourier transform of the corresponding time propagator. The T matrix for resonant vibrational excitation can then be written as

$$\begin{aligned} T_{\nu',\nu}(E) &= \frac{1}{i} \int_0^\infty dt e^{iEt} \int dR \vec{X}_{\nu'}(R)^\dagger \vec{\xi}_\nu(t, R) \\ &= \frac{1}{i} \int_0^\infty dt e^{iEt} \int dR \vec{X}_{\nu'}(R)^\dagger e^{-iHt} \vec{X}_\nu(R). \end{aligned} \quad (71)$$

This expression has the form of an overlap of a two-component wave packet propagating on the coupled resonance surfaces, whose initial condition is determined by the the entry amplitude

$$\vec{X}_\nu(R) = \begin{pmatrix} [\Gamma_1(R)/2\pi]^{1/2} \chi_\nu(R) \\ [\Gamma_2(R)/2\pi]^{1/2} \chi_\nu(R) \end{pmatrix}, \quad (72)$$

with a stationary vector exit amplitude of the same form, but corresponding to the final vibrational state ν' .

In Eq. (71) the interval $[0, \infty)$ of the time integration is determined by the boundary conditions satisfied by Green's function in Eq. (30). The time-dependent formulation gives an appealing picture of the physics of a collision, in which the resonant attachment of the incident electron creates a wave packet on the resonant surfaces that moves while decaying due to the finite lifetime of the resonance. The familiar “boomerang” structure in the vibrational excitation cross sections can arise if the wave packet survives on the complex potential surfaces long enough to revisit its original location and cause at least one “recurrence” in the time-dependent overlap in Eq. (71).

To construct the integral and differential cross sections we need the individual t_{ij} amplitudes. The time-dependent representation for t_{ij} , which is apparent from Eq. (71), is

$$\begin{aligned} t_{i,j}(E) &= \frac{1}{i} \int_0^\infty dt e^{iEt} \int dR \begin{pmatrix} \delta_{i1} & 0 \\ 0 & \delta_{i2} \end{pmatrix} \vec{X}_{\nu'}(R)^\dagger \\ &\quad \times e^{-iHt} \begin{pmatrix} \delta_{j1} & 0 \\ 0 & \delta_{j2} \end{pmatrix} \vec{X}_\nu(R). \end{aligned} \quad (73)$$

The four t_{ij} amplitudes are thus found by starting the wave packet on one or the other of the 2A_1 or 2B_1 surfaces, specified by the index j , and Fourier transforming its overlap with an exit amplitude on the surface specified by i .

For systems with more than one vibrational degree of freedom, the time-dependent formulation provides a computational advantage, because it does not involve the solution of large systems of complex linear equations. The propagation times in this problem are generally short, since the wave packets survive on the complex surfaces for at most a few vibrational periods. In these calculations the propagation times varied from 35 to 50 fs, depending on the initial conditions, at which point the norm of the packets was negligibly small and the t_{ij} amplitudes in Eq. (73) were converged. As in our earlier study on this system [10], we have chosen to propagate the wave packets using the multiconfiguration time-dependent Hartree (MCTDH) method [16,32].

The underlying discretization of s_1 and ρ was made using a discrete variable representation (DVR) for each degree of freedom. The “standard” method for solving the time-dependent Schrödinger equation would construct an explicit solution for the packet propagating on the multidimensional DVR grid. A serious problem with this approach is that the computational effort required scales exponentially with the number of degrees of freedom, making it prohibitively expensive to implement as the number of degrees of freedom grows. The MCTDH method retains the essential rigor of the standard method while providing extraordinary computational efficiency, especially for systems with many degrees of freedom.

In the MCTDH method, as in the standard method, we start with a time-independent orthonormal product basis set,

$$\{\chi_{j_1}^{(1)}(Q_1) \cdots \chi_{j_f}^{(f)}(Q_f)\}, \quad j_\kappa = 1, \dots, N_\kappa, \quad (74)$$

where we have assumed that there are f degrees of freedom in a problem described by nuclear coordinates Q_1, \dots, Q_f . For computational efficiency, the basis functions, $\chi_{j_\kappa}^{(\kappa)}$, are chosen as the basis functions of a discrete variable representation (DVR) [33].

The central idea in the MCTDH scheme [16,34,35] is that one can employ a smaller, but now time-dependent, basis for expanding the wave function, i.e.,

$$\Psi(Q_1, \dots, Q_f, t) = \sum_{j_1=1}^{n_1} \cdots \sum_{j_f=1}^{n_f} A_{j_1, \dots, j_f}(t) \prod_{\kappa=1}^f \varphi_{j_\kappa}^{(\kappa)}(Q_\kappa, t) \quad (75)$$

with $n_\kappa \ll N_\kappa$. The single-particle functions in turn are represented as linear combinations of the primitive basis in Eq. (74),

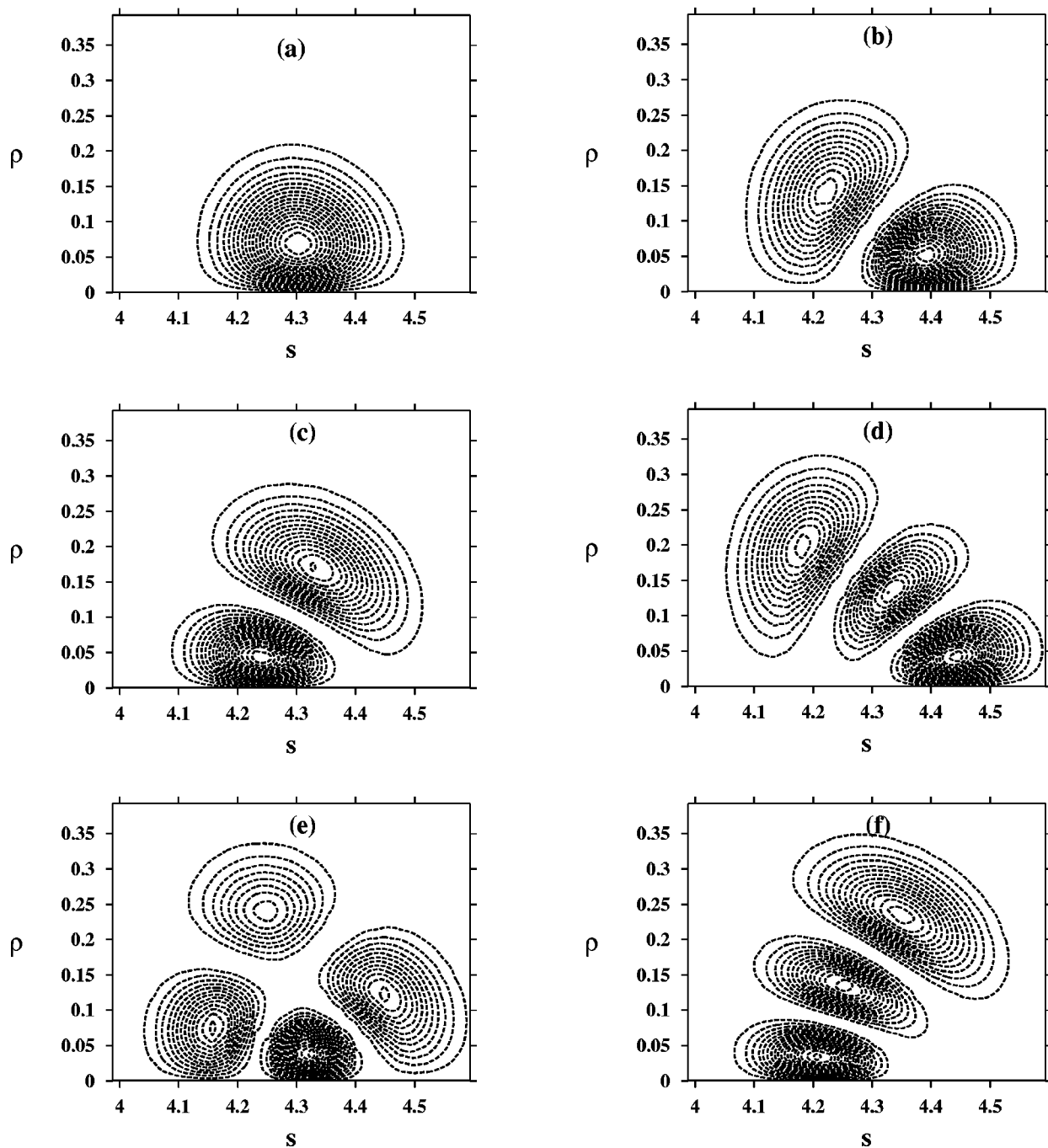


FIG. 3. Vibrational wave functions calculated on the SCF surface (times bending normal coordinate $\rho^{1/2}$). (a) Ground state, (b) lower member of Fermi dyad, (c) upper member of dyad, (d) lowest member of Fermi triad, (e) middle member of triad, (f) highest member of triad. The normal coordinates ρ and s are in atomic units.

$$\varphi_{j_\kappa}^{(\kappa)}(Q_\kappa, t) = \sum_{i_\kappa=1}^{N_\kappa} c_{i_\kappa j_\kappa}^{(\kappa)}(t) \chi_{i_\kappa}^{(\kappa)}(Q_\kappa). \quad (76)$$

Since both the coefficients, $A_{j_1 \dots j_p}$, and the single-particle functions are time dependent, the wave-function representation is not unique. Uniqueness can be achieved by imposing additional constraints on the single-particle functions which keep them orthonormal for all times [16].

The MCTDH approach has been applied to a variety of problems ranging from reactive and surface scattering to the determination of photodissociation and photoabsorption spectra (see Ref. [16] and references therein). The success of this method for systems with a large number of degrees of freedom was underlined in a recent application to the spin-boson model including 80 vibrational modes [36]. We used this approach in our earlier calculations on CO₂ which involved only the ²A₁ resonance state [10] and found that it works very effectively for propagation on complex potential

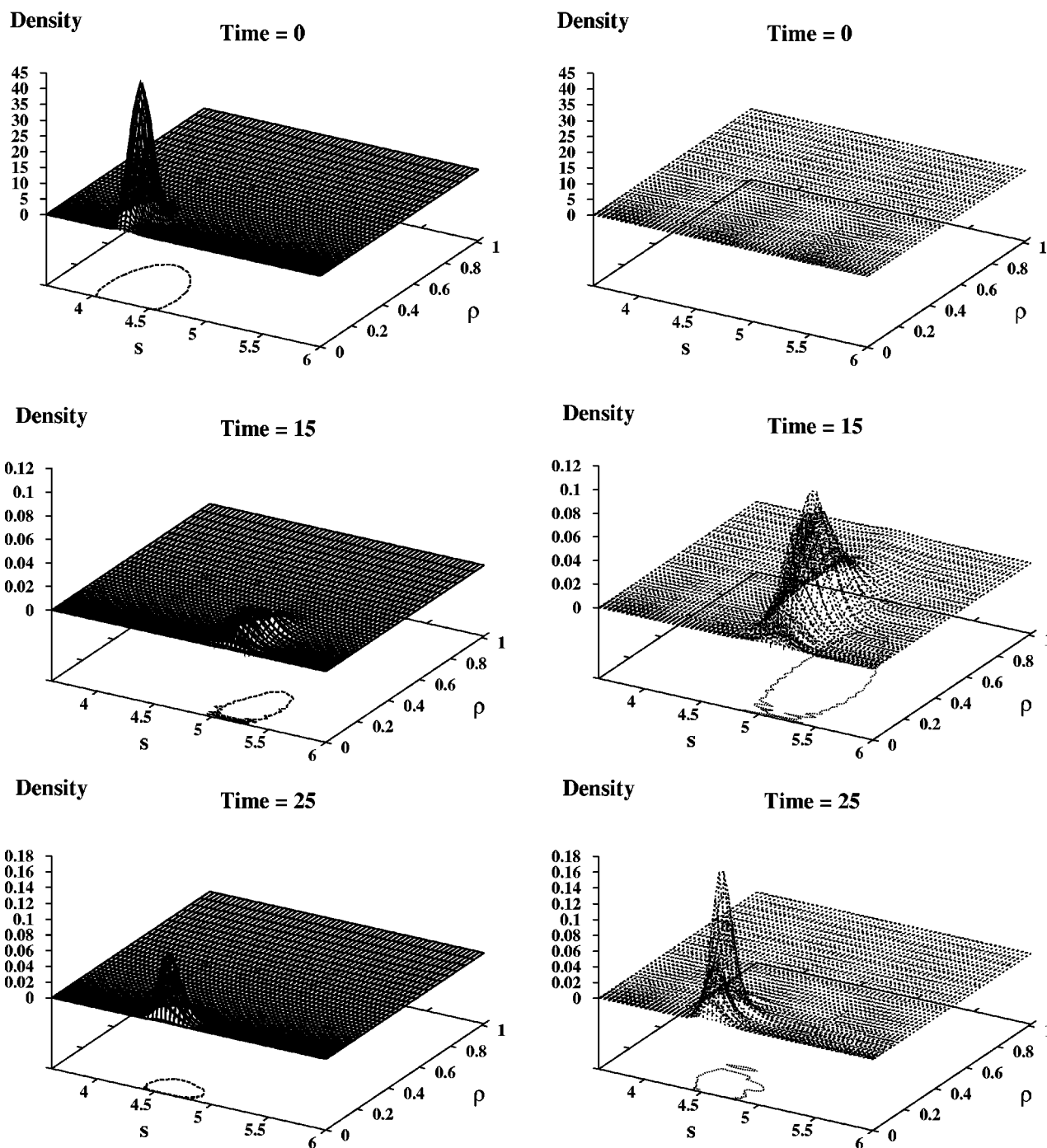


FIG. 4. Wave-packet propagation beginning at 2A_1 (lower) resonance surface. All quantities are in atomic units. Left column, component of packet on 2A_1 surface; right column, component of packet on 2B_1 surface.

surfaces. Applying the MCTDH approach in this case requires that we reexpress our representation of the potentials as sums of separable terms, but that expansion can be accomplished without difficulty. MCTDH is particularly useful for solving problems with many degrees of freedom. However, it can be very convenient to use MCTDH even for rather low-dimensional problems, as the MCTDH package [32] supplies analysis routines (e.g., evaluation of cross correlation) and visualization routines which work in conjunction with the propagation routine.

The Renner-Teller Hamiltonian in Eq. (69) presents a problem that we did not encounter in our earlier study. Previously, we used Cartesian normal coordinates in our representation of the Hamiltonian for the 2A_1 resonance state. In that representation, the Hamiltonian is three dimensional. In the present case of the two-component Renner-Teller Hamiltonian, with N_z and L_z quantized, the representation is two dimensional. However, the Renner-Teller Hamiltonian has singularities of the form $1/\rho^2$ at the origin of the bending coordinate, both in the diagonal and coupling terms. The

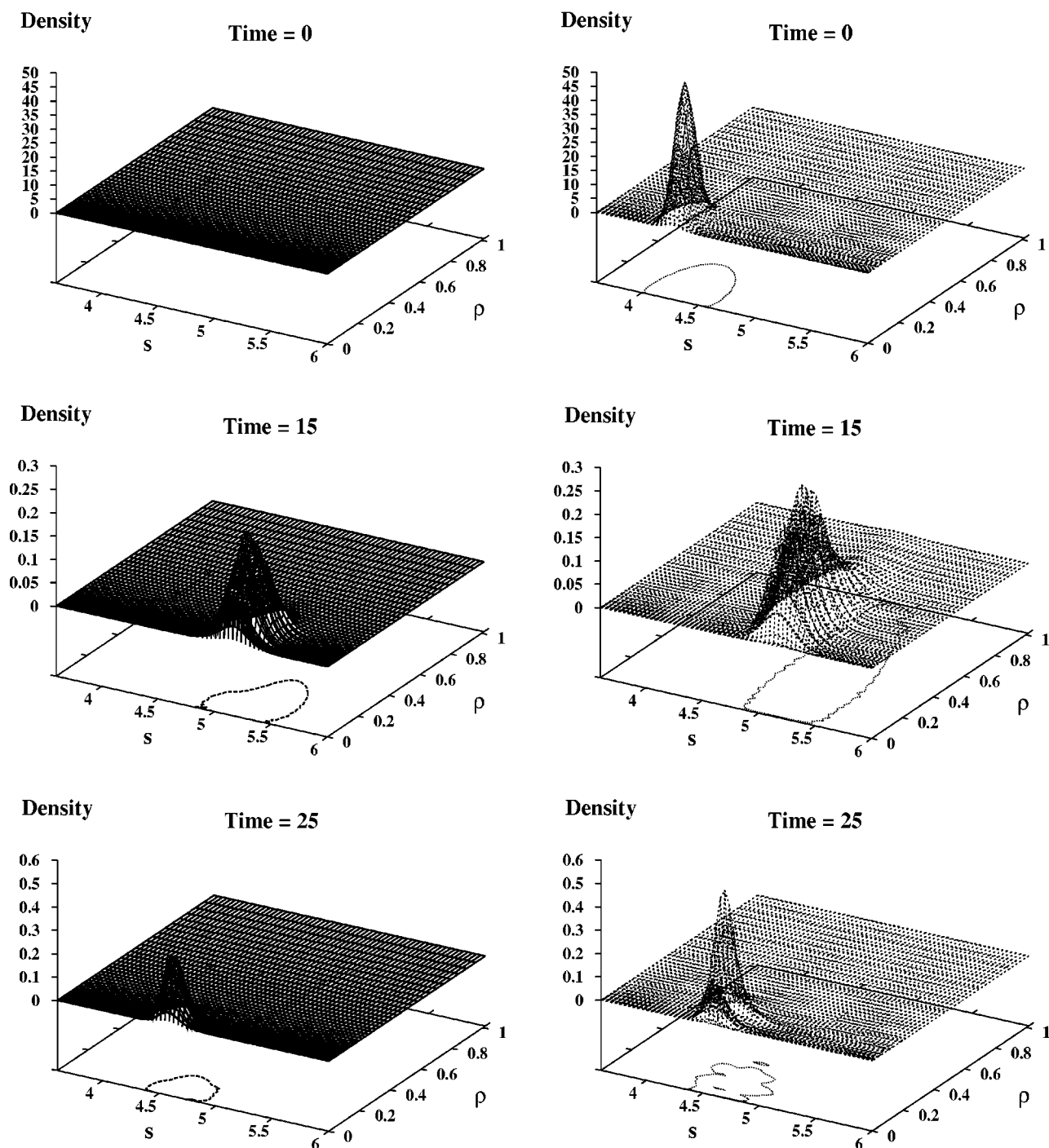


FIG. 5. Wave-packet propagation beginning at 2B_1 (upper) resonance surface. All quantities are in atomic units. Left column, component of packet on 2A_1 surface; right column, component of packet on 2B_1 surface.

stretching motion can be treated with any one of several well-known choices of DVR (sin, Hermite, etc.), because the potentials cause the packet to vanish benignly at the limits of the grid in s_1 . On the other hand, the ρ motion requires a modified DVR to treat the singularity at $\rho=0$ properly.

The problem of the singularity in ρ appears even in the Schrödinger equation for nuclear motion on the ${}^1\Sigma_g$ ground state of CO_2 when the bending motion is expressed in these coordinates,

$$H = -\frac{1}{2\mu_1} \frac{\partial^2}{\partial s_1^2} - \frac{1}{2\mu_2} \frac{\partial^2}{\partial \rho^2} + \frac{1}{2\mu_2 \rho^2} \left(K^2 - \frac{1}{4} \right) + V(s_1, \rho). \tag{77}$$

The eigenstates of this Hamiltonian behave as $\rho^{K+1/2}$ at the origin and thus their derivatives with respect to ρ diverge at $\rho=0$. If coupling is neglected in the Renner-Teller matrix Hamiltonian, the behavior at the origin of the wave function

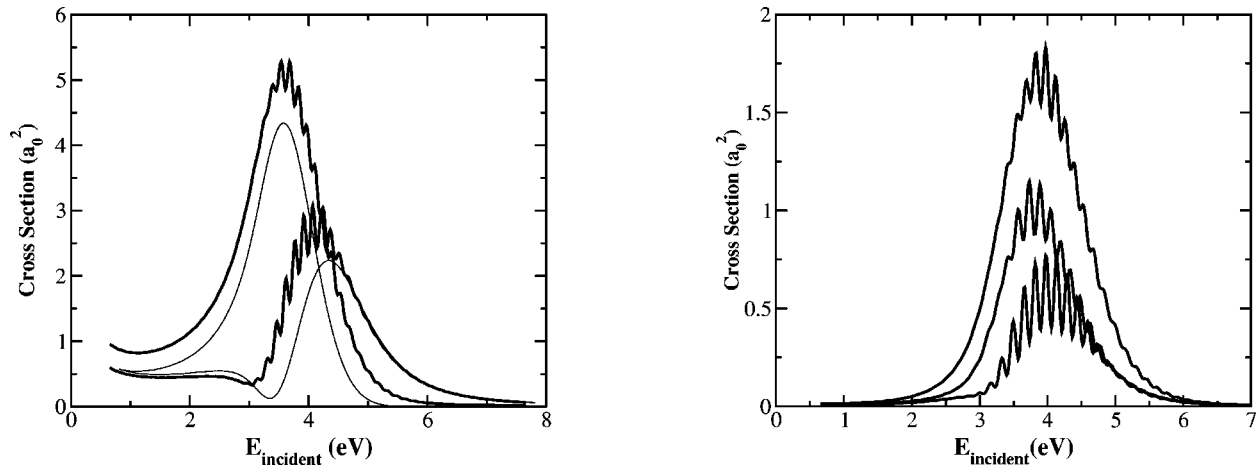


FIG. 6. Integral cross sections for vibrational excitation. Left panel: Fermi dyad, upper heavy solid line denotes high-energy component of dyad, lower heavy solid line denotes low-energy component of dyad, light solid lines are the results of earlier calculations from Ref. [10]. Right panel: Fermi triad, heavy solid lines in order of decreasing magnitude denote high-, middle and low-energy members of triad.

is $\rho^{1/2 + \sqrt{K^2 + \Lambda^2}}$. Since we must consider the case of $K=0$ for the initial and final vibrational states, we require a DVR that allows the wave function to behave as $\rho^{1/2}$ at the origin, and thus take on the most singular behavior for its derivative, $\rho^{-1/2}$, that our numerical calculations on the propagating wave packets can encounter. The problem was solved by adopting a Laguerre DVR with underlying basis functions ϕ that satisfy the boundary condition $\phi(\rho) \sim \rho^{1/2}$. This Laguerre DVR is described in the Appendix.

VI. CROSS SECTIONS FOR EXCITATION OF LOWEST FERMI DYAD AND TRIAD VIBRATIONAL STATES OF CO₂

As we emphasized in our earlier single-channel study [10], the near degeneracy of the zeroth-order symmetric stretch and bending levels ($\nu_{stretch} \approx 2\nu_{bend}$), or “Fermi resonance” phenomenon, leads to a complete breakdown of the single-mode description of the excited vibrational states. The classic approach to this problem is to describe the vibrational states as linear combinations of the zeroth-order single-mode levels using degenerate perturbation theory. This was the procedure we previously employed [10], using the semiempirically determined values for the mixing coefficients given in Dennison’s classic work [14]. In the present work, we have opted for a completely *ab initio* approach and so the target vibrational states were computed numerically using the 2D Hamiltonian of Eq. (70) and our calculated SCF results potential surface. Figure 3 shows contour plots of the “radial” wave functions, Φ [Eq. (56)], for the ground state and for the various components of the Fermi-coupled dyad and triad. Note that, because of the boundary conditions, these functions vanish at linear geometry, $\rho=0$, as explained above. The striking thing to notice here is how the nodal lines for the upper and lower members of each polyad curve in opposite directions, the upper levels favoring a “stretched and bent” target configuration.

All of the calculations we are reporting are for excitation of CO₂ starting in its ground vibrational state. This state,

multiplied by either $(\Gamma_{A_1}/2\pi)^{1/2}$ or $(\Gamma_{B_1}/2\pi)^{1/2}$, becomes the initial wave packet for a time-dependent propagation using the techniques previously outlined. Figures 4 and 5 show how the wave packets evolve on the two surfaces when they are initiated on either the 2A_1 or 2B_1 surface, respectively. In the first case, the component of the wave packet on the 2A_1 surface rapidly vanishes as it spreads because of the dramatic increase in the width associated with increased bending. As the 2A_1 component dissipates, population density on the 2B_1 starts to build up but, because of the relatively constant behavior of the width on the 2B_1 surface, is not rapidly extinguished. Figure 5 shows the case when the wave packet is initiated on the 2B_1 surface. Once again, the population density on the 2B_1 surface broadens as the anion bends and stretches, but a significant fraction survives after a single recurrence time. In contrast, the population fraction that appears on the lower 2A_1 surface is rapidly quenched.

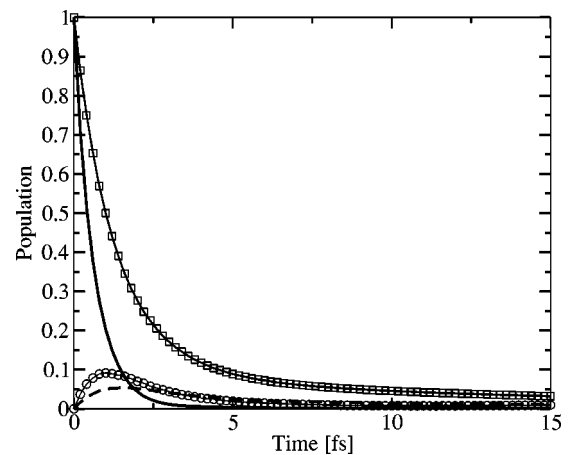


FIG. 7. Populations of the 2A_1 and 2B_1 resonance states during propagation of wave packets. For packet beginning at 2A_1 : solid curve denotes population of 2A_1 and dashed curve denotes population of 2B_1 . For the packet beginning at 2B_1 : solid curve with squares denotes population of 2B_1 and solid curve with circles denotes population of 2A_1 .

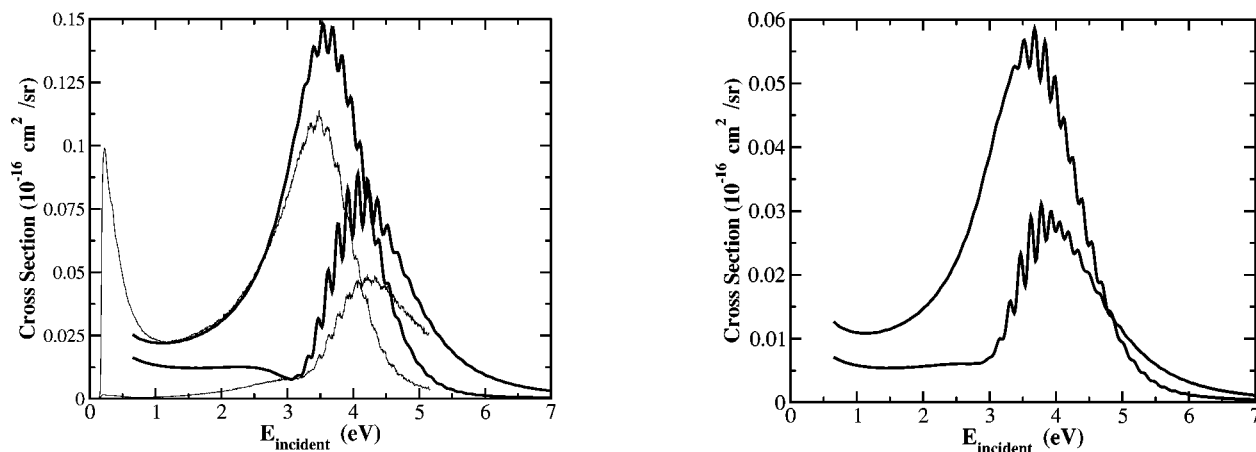


FIG. 8. DCS for vibrational excitation of the Fermi dyad. Left panel: 135° , upper (lower) heavy solid curve denotes high- (low-) energy member of dyad, light curves denote absolute experimental values of Ref. [4]. Right panel: calculated DCS at 90° , upper (lower) curve denotes high- (low-) energy member.

The integral cross sections for excitation of the Fermi-coupled dyad and triad levels were computed as described above and are shown in Fig. 6. Comparing these cross sections with our earlier results for the dyad [10], we find that the inclusion of the 2B_1 component of the resonance gives rise to the interference structure in the cross sections, which was entirely absent in the earlier one-channel treatment. Indeed, the structure is seen to be most pronounced in the energy ranges where the individual levels of each polyad strongly overlap, for example, on the high-energy side of the upper Fermi dyad and the low-energy side of the lower Fermi dyad cross sections. These boomerang structures require that a component of the wave packet survive for at least a single vibrational period on the negative-ion surfaces and in this case are clearly associated with the B_1 resonance component. The dominance of B_1 at longer times is evident from the time dependence of the electronic-state populations shown in Fig. 7.

Another noteworthy feature of these results is that there is evidently a correlation between the magnitude of the cross sections and the structure of the target vibrational levels. For both the dyad and the triad, it is the highest-energy member of each polyad that has the largest excitation cross section which in turn corresponds, as seen in Fig. 3, to the vibrational state that “leans” toward larger s (stretching coordinate). The signatures of the Fermi resonance states are thus seen in the magnitudes of the cross sections.

Using the t_{ij} amplitudes, we computed the differential cross sections given by Eq. (45). The results for the dyad are shown in Fig. 8. The left panel of this figure compares our calculated cross section with Allan’s [4] absolute differential cross sections at 135° . We note that the calculations are successful in reproducing both the overall energy dependence and fine structure in the cross sections, while the peak values of the cross section are approximately 50% larger than the measured values. We hasten to point out that the boomerang model assumption that the angular dependence of the resonance states can be described by a single partial wave is not very realistic in the present case, where bending changes the symmetry of the target. For this reason, we feel that the

absolute magnitudes of the integrated cross sections are probably more accurate than the differential results. The right panel of Fig. 8 shows the calculated values at 90° . The calculations predict that the magnitude of the cross sections at 90° is roughly half of what it is at 135° , whereas the ratio of the upper to lower dyad cross sections is about the same.

Our calculated results for the triad at 90° and 135° are shown in Fig. 9. Here, the importance of the interference term in Eq. (25) for the differential cross section is more noticeable: the relative magnitudes of the individual levels depend strongly on the scattering angle. Finally, in Fig. 10, we compare our calculated cross section for excitation of the highest level of the triad with the results reported by Allan at 90° [5]. The measurements in this case are not absolute, and were therefore scaled for comparison with our calculations. Here we note that a shift of a few tenths of an eV in the energy scale, which reflects our error in the absolute placement of the anion state relative to the neutral, brings theory and experiment into essentially perfect qualitative agreement.

VII. DISCUSSION

We have attempted to demonstrate with this study that resonant vibrational excitation in an electron-polyatomic molecule collision can be accurately treated entirely from first principles. In the present case of CO_2 , that goal has been largely achieved. Moreover, the treatment highlights aspects of the collision dynamics that give rise to observable effects that are purely polyatomic in nature. We have seen how the phenomenon of Fermi resonance makes a multidimensional treatment of the nuclear dynamics essential and how the different members of a Fermi polyad imprint their unique signatures on the vibrational excitation cross sections. Moreover, the fact that the resonance state, which is doubly degenerate when the target is in its initial linear geometry, splits into two nondegenerate components when the molecule bends, leads naturally to a coupled-channel generalization of the complex local potential or boomerang model, with nonadiabatic Coriolis coupling providing the mecha-

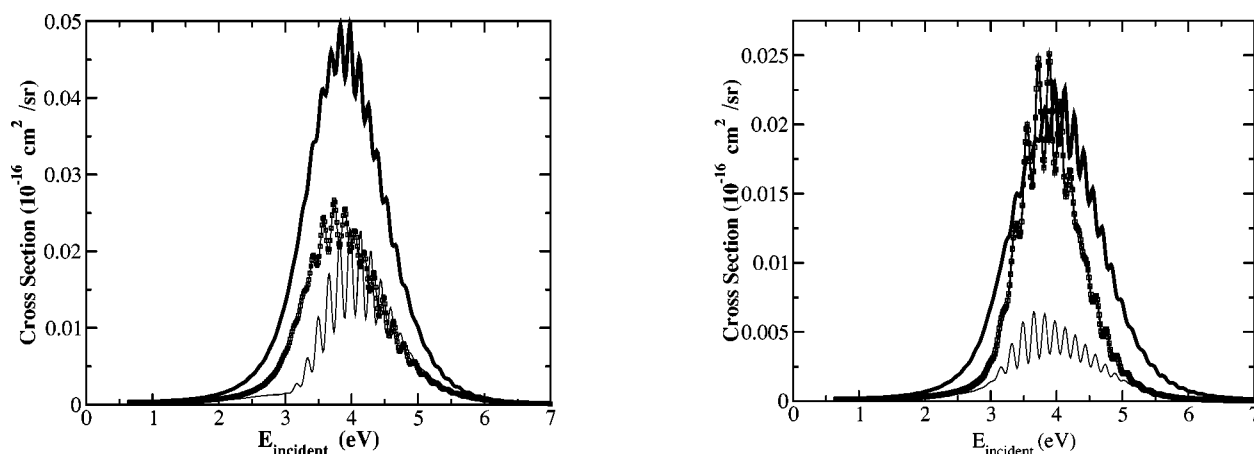


FIG. 9. Calculated DCS for vibrational excitation of the Fermi triad. Heavy solid curve, high-energy member; solid curve with squares, middle member; light solid curve, low-energy member. Left panel, 135°; right panel, 90°.

nism for coupling the dynamics on the two resonance surfaces. That coupling is essential to include if we are to describe the fine structure in the cross sections.

Our treatment only takes symmetric stretch and bending motion into consideration. Asymmetric stretch is probably needed for a better quantitative description, although Kazanskii's recent model calculations have investigated such effects and found them to be small [11]. We have restricted our calculations to excitations from the ground vibrational state into the first two Fermi polyads, where we expect that the coupled-channel boomerang treatment captures the essential physics. The local complex potential approach will probably break down radically when the dynamics probes parts of the 2A_1 surface where it crosses (or avoids crossing) the ground state of the anion. That crossing (or avoided crossing) occurs for symmetric stretch near equilibrium but with large bending angles, which would be probed by the dynamics of vibrational excitation either ending or starting with highly excited vibrational levels.

The resonance formalism we have used cannot describe “forbidden” processes such as excitation of nontotally symmetric vibrational levels from the ground state, as Currell

and Comer have implied [8] in citing the work of Estrada *et al.* [15]. The situation described by Estrada *et al.* pertains to the vibronic coupling, in polyatomic molecules belonging to Abelian point groups, between resonance states belonging to totally symmetric and nontotally symmetric representations, respectively. For the $^2\Pi_u$ Renner-Teller situation we have considered here, such transitions are still forbidden by symmetry. On the other hand, a traditional adiabatic-nuclei treatment [37] that included bending (instantaneous symmetry breaking) would give a nonzero cross section for such transitions, since the dipole moment induced by bending couples even and odd components of the total wave function. Rathbone *et al.* [38] have studied this mechanism in connection with CO₂ photoionization and have shown that it can produce large cross sections when enhanced by a shape resonance. This mechanism, however, would not explain the interference structures in the cross sections for such transitions that are clearly seen in Allan's measurements [4]. A proper theoretical treatment of this problem remains an open question.

There are also unanswered questions associated with structures that have been observed [5] in the excitation cross sections for certain vibrational levels in the energy region below 1 eV. For example, the mechanism that produces boomeranglike vibrational structure near threshold in the excitation cross sections for the upper levels of the higher polyads is still not established, but an interaction or interference of the virtual state [19] with the resonant state dynamics is likely to play a major role. As we discussed in our recent model study [20], however, the topology of that virtual state or resonance surface has a complicated structure for reasons associated with the angle-dependent dipole moment of the target. The observed structure is reminiscent of what has been seen previously [39] in threshold vibrational excitation of HCl, and that structure has been successfully treated in *ab initio* “nonadiabatic *R*-matrix” calculations [40]. However, the multidimensional nature of the nuclear dynamics involved in the present case would likely make a straightforward extension of that approach quite difficult. A complete theoretical study of vibrational excitation outside the resonance region remains a formidable challenge.

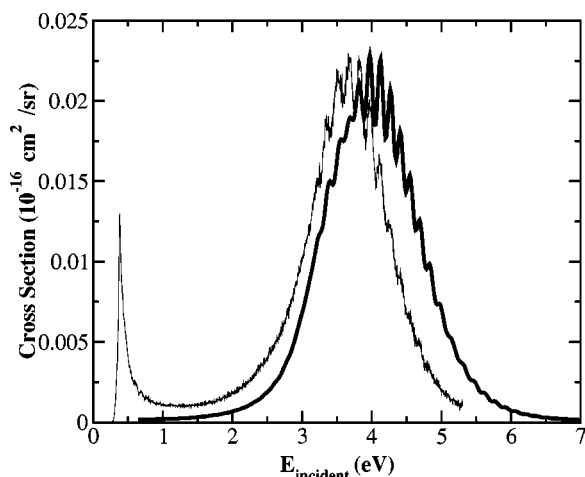


FIG. 10. Differential cross section for the high-energy member of Fermi triad at 90° (heavy solid curve) compared with relative DCS of Ref. [5].

ACKNOWLEDGMENTS

This work was performed under the auspices of the U.S. Department of Energy by the University of California Lawrence Berkeley and Lawrence Livermore National Laboratories under Contract Nos. DE-AC03-76SF00098 and W-7405-Eng-48, respectively. The work was supported by the U.S. DOE Office of Basic Energy Science, Division of Chemical Sciences, and computations were carried out at the National Energy Research Scientific Computing Center at Lawrence Berkeley National Laboratory. H.D.M. gratefully acknowledges support through the ‘‘DFG Forschergruppe: Schwellenverhalten, Resonanzen und nichtlokale Wechselwirkungen bei niederenergetischen Streuprozessen.’’

APPENDIX: LAGUERRE DVR

As finite basis set representation (FBR) underlying the DVR we use the functions

$$\phi_n^a(x) = \sqrt{\frac{(n-1)!}{(n+a-1)!}} x^{a/2} e^{-x/2} L_{n-1}^a(x), \quad (\text{A1})$$

where

$$L_n^a(x) = \frac{1}{n!} e^x x^{-a} \frac{d^n}{dx^n} (e^{-x} x^{n+a}) \quad (\text{A2})$$

is the generalized Laguerre polynomial and $a=1,2,3,\dots$. Note that in Eq. (A1) and in the following $n=1,2,\dots,N$, where N denotes the number of basis functions (or number of DVR points) taken into account. The basis functions satisfy the boundary condition $\phi_n^a(x) \sim x^{a/2}$ for $x \rightarrow 0$, they are orthonormal on the interval $[0,\infty)$,

$$\int_0^\infty \phi_n^a(x) \phi_m^a(x) dx = \langle \phi_n^a | \phi_m^a \rangle = \delta_{nm}, \quad (\text{A3})$$

and satisfy the recurrence relation

$$\begin{aligned} x \phi_n^a(x) &= -\sqrt{(n-1)(n+a-1)} \phi_{n-1}^a(x) + (2n+a-1) \\ &\times \phi_n^a(x) - \sqrt{n(n+a)} \phi_{n+1}^a(x). \end{aligned} \quad (\text{A4})$$

This recurrence relation defines the matrix representation of the position operator. Diagonalization of the position operator matrix produces the DVR points, which are given by the eigenvalues, and the FBR/DVR transformation matrix \mathbf{U} , which is the eigenvector matrix of $\langle \phi_n^a | x | \phi_m^a \rangle$. As the latter matrix is tridiagonal, one knows that the present DVR is a ‘‘proper’’ DVR, i.e., the potential matrix element evaluation is equivalent to a Gaussian quadrature rule. (See e.g. Ref. [33] or Appendix B of Ref. [16].)

Next we have to determine the matrix representations of the first- and second-order derivative operators. After a considerable amount of algebra one obtains

$$D_{nm}^{(1)} = \left\langle \phi_n^a \left| \frac{d}{dx} \right| \phi_m^a \right\rangle = \frac{1}{2} v_{nm} w(n,m,a) \quad (\text{A5})$$

and

$$\begin{aligned} D_{nm}^{(2)} &= \left\langle \phi_n^a \left| \frac{d^2}{dx^2} - \frac{c}{x^2} \right| \phi_m^a \right\rangle = -\frac{2n_{<} + a - 1}{2(a+1)} w(n,m,a) \\ &+ \frac{1}{4} \delta_{nm}, \end{aligned} \quad (\text{A6})$$

where

$$v_{nm} = \begin{cases} -1 & \text{if } n < m, \\ 0 & \text{if } n = m, \\ 1 & \text{if } n > m \end{cases} \quad (\text{A7})$$

and

$$w(n,m,a) = \sqrt{\frac{(n_{<} + a - 1)!(n_{>} - 1)!}{(n_{<} - 1)!(n_{>} + a - 1)!}}, \quad (\text{A8})$$

with $n_{<} = \min(n,m)$ and $n_{>} = \max(n,m)$, and

$$c = \begin{cases} K^2 - 1/4 & \text{with } K = (a-1)/2 \text{ if } a = \text{odd}, \\ j(j+1) & \text{with } j = (a-2)/2 \text{ if } a = \text{even}. \end{cases} \quad (\text{A9})$$

Hence $c = -1/4, 0, 3/4, 2$ for $a = 1, 2, 3, 4$. Note that c/x^2 is the centrifugal potential for cylindrical ($a = \text{odd}$) or spherical ($a = \text{even}$) symmetry.

For sake of completeness we also give the matrix elements of the first two inverse powers.

$$I_{nm}^{(1)} = \langle \phi_n^a | x^{-1} | \phi_m^a \rangle = a^{-1} w(n,m,a) \quad (\text{A10})$$

and

$$\begin{aligned} I_{nm}^{(2)} &= \langle \phi_n^a | x^{-2} | \phi_m^a \rangle \\ &= \frac{(a-2)!}{(a+1)!} [(a+1)n_{>} - (a-1)(n_{<} - 1)] w(n,m,a), \end{aligned} \quad (\text{A11})$$

where the latter equation is valid for $a \geq 2$ only.

The matrix (A5) can now be transformed to DVR representation

$$\mathbf{D}^{(1),\text{DVR}} = \mathbf{U}^\dagger \mathbf{D}^{(1)} \mathbf{U} \quad (\text{A12})$$

and similarly for $\mathbf{D}^{(2)}$, $\mathbf{I}^{(1)}$, and $\mathbf{I}^{(2)}$. The matrices (A10) and (A11) are not needed, in principle, because potential terms are usually evaluated by the DVR approximation, which is equivalent to evaluating Eqs. (A10) and (A11) by a particular Gaussian quadrature (where the DVR points are the quadrature points). However, due to the singularity at $x=0$, the quadrature is not very accurate, and, when a high precision is needed, one may want to use Eqs. (A10) and (A11), or their DVR-transformed versions, respectively.

Two remarks are finally necessary. First, the variable x is to be replaced in actual calculations by r/r_0 (or ρ/ρ_0), where the length scale r_0 has to be chosen appropriately. (This is similar to adjusting the frequency parameter ω in a Hermite DVR.) Second, the Laguerre DVR shows a *very* uneven distribution of DVR points. The points are much more dense close to the origin and become wider spaced for larger x . As a consequence, the second derivative matrix has very large negative eigenvalues, i.e., the kinetic-energy operator, and hence the Hamiltonian will have very large eigenvalues. Most integrators for the time-dependent Schrödinger equation, however, are sensitive to large eigenvalues. The step-size taken is proportional to the inverse of the largest modu-

lus of the eigenvalues of the Hamiltonian. Hence, large potential values are usually removed by simply truncating the potential at some appropriate value. To make the Laguerre DVR useful for wave-packet propagation, we follow a similar route. The second derivative matrix, Eq. (A6) is diagonalized, and the large negative eigenvalues are dropped beyond some appropriate value. Using these modified eigenvalues, the diagonal matrix is backtransformed to its original representation. Our experience with this modification of the kinetic-energy operator was very satisfactory. To give some typical numbers, out of 50 eigenvalues we dropped 5 or 6. The integration step size increased by about a factor of 30, but the errors introduced by the modification remained negligible.

-
- [1] Brücke, Ann. Phys. (Leipzig) **83**, 1065 (1927).
 [2] I. Cadez, F. Greteau, M. Tronc, and R.I. Hall, J. Phys. B **10**, 3821 (1977).
 [3] W.M. Johnstone, P. Akther, and W.R. Newell, J. Phys. B **28**, 743 (1995).
 [4] M. Allan, Phys. Rev. Lett. **87**, 033201 (2001).
 [5] M. Allan, J. Phys. B **35**, L387 (2002).
 [6] D.T. Birtwistle and A. Herzenberg, J. Phys. B **4**, 53 (1971).
 [7] L. Dube and A. Herzenberg, Phys. Rev. A **20**, 194 (1979).
 [8] F. Currell and J. Comer, J. Phys. B **26**, 2463 (1993).
 [9] G. Herzberg, *Molecular Spectra and Molecular Structure II. Infrared and Raman Spectra of Polyatomic Molecules* (Van Nostrand Reinhold, New York, 1945).
 [10] T.N. Rescigno, W.A. Isaacs, A.E. Orel, H.-D. Meyer, and C.W. McCurdy, Phys. Rev. A **65**, 032716 (2002).
 [11] A.K. Kazanskii, Opt. Spectra **87**, 840 (1999).
 [12] T.N. Rescigno, D.A. Byrum, W.A. Isaacs, and C.W. McCurdy, Phys. Rev. A **60**, 2186 (1999).
 [13] C.W. McCurdy and J.L. Turner, J. Chem. Phys. **78**, 6773 (1983).
 [14] D.M. Dennison, Rev. Mod. Phys. **12**, 175 (1940).
 [15] H. Estrada, L.S. Cederbaum, and W. Domcke, J. Chem. Phys. **84**, 152 (1986).
 [16] M.H. Beck, A. Jäckle, G.A. Worth, and H.-D. Meyer, Phys. Rep. **324**, 1 (2000).
 [17] D.G. Hopper, Chem. Phys. **53**, 85 (1980).
 [18] G.L. Gutsev, R.J. Bartlett, and R.N. Compton, J. Chem. Phys. **108**, 6756 (1998).
 [19] The existence of a virtual state in the electron-CO₂ system was first proposed by M.A. Morrison, Phys. Rev. A **25**, 1445 (1984), and was subsequently the subject of numerous semi-empirical studies. The first *ab initio* calculation to confirm the virtual state mechanism was by L.A. Morgan, Phys. Rev. Lett. **80**, 1873 (1998); a recent theoretical analysis is given by Mazevet *et al.*, Phys. Rev. A **64**, 040701(R) (2001).
 [20] W. Vanroose, C.W. McCurdy, and T.N. Rescigno, Phys. Rev. A **66**, 032720 (2002).
 [21] H. Feshbach, Ann. Phys. (N.Y.) **19**, 287 (1962).
 [22] A.U. Hazi, T. Rescigno, and M. Kurilla, Phys. Rev. A **23**, 1089 (1981).
 [23] A.U. Hazi, A.E. Orel, and T.N. Rescigno, Phys. Rev. Lett. **46**, 918 (1981).
 [24] C. Mundel, M. Berman, and W. Domcke, Phys. Rev. A **32**, 181 (1985).
 [25] G.A. Gallup, Y. Xu, and I.I. Fabrikant, Phys. Rev. A **57**, 2596 (1998).
 [26] F.H. Mies, Phys. Rev. **175**, 164 (1968).
 [27] A.U. Hazi, J. Phys. B **16**, L29 (1983).
 [28] A.R. Edmonds, *Angular Momentum in Quantum Mechanics* (Princeton University Press, Princeton, 1960).
 [29] R. Renner, Z. Phys. **92**, 172 (1934).
 [30] J.M. Brown and F. Jorgensen, Adv. Chem. Phys. **52**, 117 (1982).
 [31] C. Jungen and A.J. Merer, Mol. Phys. **40**, 1 (1980).
 [32] G.A. Worth, M.H. Beck, A. Jäckle, and H.-D. Meyer, The MCTDH Package, Version 8.2, 2000. See <http://www.pci.uni-heidelberg.de/tc/usr/mctdh/>.
 [33] J.C. Light, in *Time-Dependent Quantum Molecular Dynamics*, edited by J. Broeckhove and L. Lathouwers (Plenum, New York, 1992).
 [34] H.-D. Meyer, U. Manthe, and L.S. Cederbaum, Chem. Phys. Lett. **165**, 73 (1990).
 [35] U. Manthe, H.-D. Meyer, and L.S. Cederbaum, J. Chem. Phys. **97**, 3199 (1992).
 [36] H. Wang, J. Chem. Phys. **113**, 994 (2000).
 [37] D.M. Chase, Phys. Rev. **104**, 838 (1956).
 [38] G.J. Rathbone, E.D. Poliakov, J.D. Bozek, and R.R. Lucchese, J. Chem. Phys. **16**, 8240 (2001).
 [39] M. Allan, M. Cizek, J. Horacek, and W. Domcke, J. Phys. B **33**, L209 (2000).
 [40] L.A. Morgan, P.G. Burke, and C.J. Gillian, J. Phys. B **23**, 99 (1990).